NASA TECHNICAL MEMORANDUM

NASA TM X-71537

NASA TM X-71537

CENTAUR STANDARD SHROUD (CSS) FULL JETTISON TEST DYNAMIC ANALYSIS

by Harold J. Kasper and Richard M. Donovan
Lewis Research Center
Cleveland, Ohio 44135

April 1974

ABSTRACT

During the Space Power Facility jettison tests at the Lewis Research Center Plum Brook Station, the non-domed half of the Centaur Standard Shroud was allowed to completely separate from its hinge connection and was caught in a horizontal catch net. A rigid body dynamic analysis that was performed to predict the half shroud motion prior to and after net contact is presented. Analytical predictions of the longitudinal and circumferential bending moments imposed on the half shroud by the catch net and the net pressure on the half shroud corrugated skin are also presented.

CENTAUR STANDARD SHROUD (CSS) FULL JETTISON TEST DYNAMIC ANALYSIS

by

Harold J. Kasper and Richard M. Donovan

SUMMARY

During the Space Power Facility Jettison Tests at the Lewis Research Center Plum Brook Station, the non-domed half of the Centaur Standard Shroud was allowed to completely separate from its hinge connection and was caught in a horizontal catch net. A rigid body dynamic analysis that was performed to predict the half shroud motion prior to and after net contact is presented. Analytical predictions of the longitudinal and circumferential bending moments imposed on the half shroud by the catch net and the net pressure on the half shroud corrugated skin are also presented.

The results of the analysis indicated that in order to keep the half shroud longitudinal and circumferential bending moments within the allowable limits, initial sole contact of the half shroud biconic nose section with the net should be avoided. The analysis also showed that the corrugation pressure was below its maximum allowable limit.

E-7943

INTRODUCTION

The function of the Centaur Standard Shroud (CSS) is to protect the Centaur and payload from the ascent environment during boost. Following exit from the sensible atmosphere when the external aerodynamic pressure is near zero, the shroud is jettisoned from the launch vehicle.

The CSS consists of two longitudinal shell halves that are individually hinged at the base to a conical adapter which is connected to the interstage adapter located between the Titan second stage and the Centaur. A pyrotechnic cutting assembly mechanically joins the two halves along the longitudinal split line and at the circumferential junction of the shroud base and the conical adapter. Jettisoning of the shroud is accomplished by actuating the pyrotechnic cutting assembly which allows the shell halves to rotate away from the payload and booster in a clamshell like fashion (see Figure 1).

During the initial phase of rotation, spring thrusters supply sufficient energy to move each shell half slightly beyond the position where its center of gravity is directly over the hinge pin. Booster acceleration then aids the jettison event by increasing the rotational velocity of the shell halves until the centrifugal force is adequate to completely separate them from the booster.

During the jettison sequence the shroud edges must clear the payload envelope. Assembly and thermal stresses imposed on the shroud prior to jettison result in deflections that may reduce the available edge clearance during jettison when the joint between the shell halves is broken and the stresses are relieved.

In order to determine that clearances are adequate and that the jettison sequence functions properly, altitude jettison tests with a heated shroud were performed at the Plum Brook Space Power Facility (SPF). The facility pressure was lowered to approximate altitude conditions for each test. In addition, for the heated jettison tests a radiant heating device was used to simulate flight aerodynamic heating prior to shroud jettison. The objectives of the tests were: (Reference: Test Requirements Document - Centaur Standard Shroud, LeRC/TCPO -33).

1. Provide data to verify the analytical tools used to predict CSS motions, trajectories and thermal stress distributions during flight conditions of ascent, both prior to jettison and during jettison.

2. Determine CSS-to-payload envelope clearance during the heated jettison tests.

3. Determine CSS hinge loads, and load distribution in the critical interstage adapter stiffeners and interface ring, during heated jettison.

4. Determine loads developed in the CSS structure caused by CSS heating.

5. Verify the functional and structural capability of the CSS to separate during heated jettison.

6. Determine the trajectory of the CSS halves during the SPF jettison tests.

7. Determine CSS shell motions during the SPF jettison tests.

8. Obtain jettison "signature" data for the TC-1 flight instrumentation.

During the SPF jettison tests, the non-domed or lighter shroud half was allowed to separate completely from its hinge and was caught in a nearly horizontal catch net. The domed or heavier shroud half remained on its hinge and was restricted to approximately twenty degrees of rotation by a nearly vertical catch net. Figures 2 and 3 show the general test set up in SPF.

The dynamic loads imposed on the shroud halves by the catch nets were required to be within prescribed allowable load limits. Prior tests requiring the partial opening of the shroud into a vertical catch net without separation from its hinges demonstrated that these partial jettison catch net loads were not detrimental. Therefore, a dynamic analysis was performed on the non-domed or completely separated shroud half only. The primary objective of the analysis was to evaluate a previously designed catch net system and to recommend minor

changes if required to parameters such as net attitude angle and net vertical location that affect the magnitude of the loads imposed on the half shroud by the catch net. Hence the particular items considered were:

1. Non-domed half shroud rigid body motion from the time of shroud separation to its final position in the catch net.

2. Longitudinal bending moments imposed on the half shroud by the catch net.

3. Circumferential bending moment imposed on the half shroud by the catch net.

4. Net strap pressure on the shroud corrugations.

CATCH NET SYSTEM

Figure 4 shows the main components of the full jettison catch net system. Two six inch diameter aluminum tubes with a high temperature nylon net, strung between them, make up the catch net. The net consists of approximately 70 lateral straps and 9 longitudinal straps of Nomex, 1.0 inch (.0254m) wide by .12 inch (.00305m) thick. The tubes and net extend the full length of the shroud. Five friction disc-type brakes are attached with stainless steel cables to each of the tubes, making a total of ten brakes in the system. The brakes are attached to a steel support structure that is fastened to the SPF chamber floor. Shroud kinetic energy is absorbed primarily by the brakes which rotate as the net moves downward. The tubes and net are formed approximately to the cylinder-cone shape of the shroud.

THEORY AND ASSUMPTIONS

Figure 5 is a schematic drawing showing the function of the shroud hinge during the jettison sequence described in Figure 1. The hinge is shown in its rest position in Figure 4(a). During the first phase of shroud separation, the rotating half of the shroud hinge pivots about the fixed hinge pin as shown in Figure 4(b). As soon as the half shroud centrifugal force overcomes the acceleration or gravitational force component, the rotating hinge half lifts off of the fixed hinge pin as shown in Figure 4(c) and theoretically the center of rotation transfers from the fixed hinge pin to the half shroud center of gravity.

In the full jettison dynamic analysis of the half shroud, the point of hinge release is an important factor that determines the angular velocity and consequently the attitude of the half shroud when it contacts the catch net. The point of hinge release can be interpreted as either of two conditions as shown in Figure 6. Case I shows hinge release occurring when the bottom of

movable hinge clevis slot is completely clear of the fixed hinge pin. Case II shows hinge release occurring when the movable hinge clevis slot is completely clear of the fixed hinge pin. For Case I, the shroud hinge release angular position from the vertical and the angular velocity at that point are less than that for Case II. Since the angular velocity about the half shroud center of gravity is constant after hinge release occurs, the Case I free fall angular velocity is less than that of Case II. Consequently, the attitude of the half shroud at net contact is different for each case.

Actual hinge release probably occurs somewhere between Case I and Case II. Therefore, the analysis included herein has been applied to both of these limit cases. Throughout the analysis, Case I is referred to as "early off" and Case II as "late off".

The assumptions used in the analysis are:

1. Rigid body plane motion.
2. Brake disc inertia effects can be neglected because of the relatively large net frame inertia effects.
3. Dynamic brake cable tension and brake torque are constant.
4. Eighty percent jettison and breakaway spring efficiency.
5. Catch net is contoured exactly to the shroud shape.
6. Net forces on the half shroud are concentrated at the brake cable attachment points.
7. The half shroud horizontal velocity component is zero after net contact.
8. There are no disconnects installed on the shroud.
9. No damping.
10. Brake cables are inelastic.
11. Longitudinal net straps and net to shroud friction can be neglected.
12. Nose thruster springs dissipate all of their energy in the work to overcome nose area friction.

ANALYSIS

The analysis is performed in two phases. The first phase is concerned with half shroud motion prior to net contact and the second phase with half shroud and net system motion after net contact.

During the first phase, the trajectory of the half shroud center of gravity with respect to the fixed hinge point and the angular position of the half shroud longitudinal axis with respect to the vertical are determined in two dimensional space. The first phase is further divided into rotation about the hinge point and subsequent rotation about the half shroud center of gravity after it separates from its hinge. Figure 7 shows the forces acting on the half shroud at the time of initial separation of the shroud halves. F_1 is the breakaway spring force and F_2 is the jettison spring force. The governing equations while the shroud half is rotating about the hinge point are

$$\Theta\,(t = o) = o \tag{1}$$

$$\dot{\Theta}\,(t = o) = o \tag{2}$$

$$\ddot{\Theta}\,(t) = \frac{1}{I_o^s}\left[-m_s g l_3 \cos\,(\Theta + \Theta_3) + F_1 l_1 \sin\,(\Theta + \Theta_1) + F_2 l_2\right] \tag{3}$$

where m_s is the half shroud mass, I_o^s is the mass moment of inertia of the half shroud about the hinge point and Θ is the angle measured about the hinge point from the horizontal plane to the half shroud base plane or the angle from the vertical to the half shroud keel line. (A complete symbol list can be found in Appendix A.) Numerical integration of equation (3) provides the angular velocity and position of the half shroud as a function of time. The coordinates of the half shroud center of gravity are determined from

$$X_{cg}^s = -l_3 \cos\,(\Theta + \Theta_3) \tag{4}$$

$$Y_{cg}^s = l_3 \sin\,(\Theta + \Theta_3) \tag{5}$$

Rotation about the hinge point continues until the centrifugal force overcomes the gravitational force component and the half shroud lifts off of its hinge pin. Once the half shroud is completely free of its hinge, it is in a state of free fall and the center of rotation transfers from the hinge pin to the half shroud center of gravity. Acceleration is due solely to gravity so that the motion is described by

$$\ddot{X}_{cg}^s = o \tag{6}$$

$$\ddot{Y}_{cg}^s = -g \tag{7}$$

$$\ddot{\Theta} = o \tag{8}$$

The horizontal and angular velocities remain constant at their hinge separation values until net contact so that

$$\dot{X}^{s}_{cg} = C_1 \tag{9}$$

$$\dot{\theta} = C_2 \tag{10}$$

Numerical integration of equations (7), (9), and (10), provide the half shroud center of gravity coordinates and angular position from the time of hinge separation to the time of net contact. From this it is possible to determine the position of the half shroud profile during free fall. The half shroud profile is defined by straight lines that are coincident with the cylindrical section, the 15 degree (.262 rad.) cone section, and the 25 degree (.436 rad.) cone section as shown in figure 8. The equations of these lines are determined at each time increment. They are of the form

$$Y = n_i X + b_i, \quad i = 1, 2, 3 \tag{11}$$

where n is the slope and b is the y intercept.

Net contact is determined by comparing the stretched net following contact with the unstretched net. Figure 9 is a diagram of a typical brake station cross section. CL is the brake cable length between the brake and net frame. NL is the net length between the net frame and the point of tangency of a line drawn from the brake centerline to the shroud circumference. The total shaped length of the net and cable is given by

$$TL = 2\left\{R\eta + \left[(ZB)^2 + (YB)^2 - R^2\right]^{\frac{1}{2}}\right\} \tag{12}$$

where η is the cable angle with the horizontal and is equal to one half of the total angle subtended by the circumferential wrap of the net around the half shroud. During free fall, the Y coordinate of the half shroud profile is calculated at each brake station using the appropriate line equation (11). A ficticious total length is calculated using equation (12) for each brake station and position of the half shroud as it approaches the net. When the total length exceeds the precalculated unstretched total length, the half shroud is considered to have made net contact at that station. Since the net forces are assumed to be concentrated at the brake cable locations, five possible contact points are available.

Figure 10 shows the analytical model used for the second phase which is concerned with half shroud and net system motion after net contact. The problem is treated as one of planar motion with varying brake cable and net vertical forces acting on the half shroud and net support tubes. Vertical force variation is due to the change in the angle η and net stretch as the half shroud sinks into the net. The two net support tubes are assumed to act as one rigid tube with five brake cable forces and five net strap forces acting on it. Each of the five brake cable forces is a combination of the pair of brake cable vertical force components

acting at that station. The net forces acting on the net support tube and the half shroud are treated in the same manner. Translation of the half shroud and net frame is due to the resultant of these forces acting at the respective centers of gravity. Rotation of the half shroud and support tube or net frame about their respective centers of gravity is due to the torque created by the applied forces.

The forces imposed on the half shroud and the net frame by the net are determined from the net stretch and the load strain curve shown in figure 11. Net stretch is the difference between the stretched and unstretched total lengths excluding the cable length. The load value obtained from figure 11 is for one net strap. This value must be multiplied by the appropriate number of net straps assumed to be associated with a particular brake cable station. For example, if the strain in the stretched net at a particular brake station is .50 inches (.0127m) per 6.0 inches (.1524m) and the number of net straps allocated to that station is 14, the total net strap tension force at that station is 14,000 pounds (62,300N). The total vertical net force acting on the half shroud and the net frame at each brake station is

$$F_i = 2F_{si}\sin\eta \qquad (i = 1 \text{ thru } 5) \tag{13}$$

where F_{si} = total net strap tension force

η = cable angle (figure 9)

The vertical acceleration of the half shroud center of gravity after net contact is

$$\ddot{Y}^s_{cg} = \frac{\sum F_i - W_s}{m_s} \tag{14}$$

where w_s = half shroud weight

m_s = half shroud mass

Angular acceleration of the half shroud about its center of gravity after net contact is given by

$$\ddot{\Theta} = \frac{(F_i\, X^s_i)}{I^s_{cg}} \tag{15}$$

where X^s_i = distance from the half shroud center of gravity to a brake cable location

I^s_{cg} = half shroud mass moment of inertia about its center of gravity

Motion of the net frame and net is influenced by the net forces and the cable forces. The brake cable forces can assume one of three values. As the frame rotates, some cables can be slack so that

$$F_{ci} = 0 \tag{16}$$

If the net force is less than that required to overcome brake friction,

$$F_{ci} = F_i + W_i^F \tag{17}$$

where F_i = total vertical net force (equation 13)

W_i^F = frame weight at brake station i

When the net force is greater than that required to overcome brake friction,

$$F_{ci} = 2F_B \sin\eta \tag{18}$$

where F_B = constant preset cable tension required to overcome brake friction

Computer program logic selects the appropriate brake cable force and the vertical acceleration of the frame and net is calculated from

$$\ddot{Y}_{cg}^F = \frac{\sum F_{ci} - \sum F_i - W_{TF}}{m_F} \tag{19}$$

where W_{TF} = total frame weight

m_F = frame mass

Angular acceleration of the frame and net is given by

$$\ddot{\Theta}_F = \frac{\sum \left[(F_{ci} - F_i - W_i^F) \quad (X_i^F) \right]}{I_F} \tag{20}$$

where X_i^F = distance from the frame center of gravity to a brake cable location

I_F = frame mass moment of inertia about its center of gravity

Equations 14, 15, 19 and 20 are numerically integrated to determine velocities and positions of the half shroud and net after net contact. Once the position of the half shroud and net are determined for a time increment, new values of net stretch and net force are calculated at each brake station and substituted into the equations of motion of the net frame and half shroud. This process is continued until the angular and translational velocity of the half shroud approach zero.

The net forces on the half shroud introduce longitudinal and circumferential bending moments. Referring to figure 12, the longitudinal bending moment at a typical section m-m forward of the half shroud center of gravity can be expressed as

$$M_{m-m} = I_{cg}\ddot{\Theta} + m\,(X_{cg} - X_m)\,(X_{cg}\ddot{\Theta} - \ddot{Y}^{s}_{cg}) + F_j\,(X_j - X_m) \qquad (21)$$

where I_{cg} = mass moment of inertia of the total mass forward of section m-m

m = total mass forward of section m-m

X_{cg} = distance from the half shroud center of gravity to the center of gravity of the total mass forward of section m-m

X_m = distance from the half shroud center of gravity to section m-m

F_j = total net force at brake stations forward of section m-m

X_j = distance from the half shroud center of gravity to brake stations forward of section m-m

$\ddot{Y}^{s}_{cg}$ = half shroud vertical acceleration

$\ddot{\Theta}$ = half shroud angular acceleration about its center of gravity

For a typical section m-m aft of the half shroud center of gravity,

$$M_{m-m} = -I_{cg}\ddot{\Theta} - m\,(X_{cg} - X_m)\,(X_{cg}\ddot{\Theta} + \ddot{Y}^{s}_{cg}) + F_j\,(X_j - X_m) \qquad (22)$$

where I_{cg} = mass moment of inertia of the total mass aft of section m-m

m = total mass aft of section m-m

X_{cg} = distance from the half shroud center of gravity to the center of gravity of the total mass aft of section m-m

X_m = distance from the half shroud center of gravity to section m-m

F_j = total net force at brake stations aft of section m-m

X_j = distance from the half shroud center of gravity to brake stations aft of section m-m

The applied ring segment circumferential bending moment is composed of a moment due to the net strap forces which tend to increase the half shroud curvature and a moment due to the deceleration forces which tend to decrease the half shroud curvature. If it is assumed that the net strap load is distributed uniformly along the strap contact length as shown in figure 13 and that the half shroud cross sectional unit weight is uniform, the circumferential bending moment for a ring segment is given by

$$M_\phi = \frac{TR}{2} \sin\eta \left[\cos\phi \ (2 - \cos\phi\ ) - 1\right] ; \quad (23)$$

$$0 \le \phi \le \left(\frac{\pi}{2} - \eta\right) \ \& \ \eta > 0$$

and,

$$M_\phi = TR \left\{ \frac{\sin\eta}{2} \left[\cos\phi \ (2 - \cos\phi\ ) - 1\right] \right. \quad (24)$$

$$\left. + 1 - \sin(\phi + \eta) \right\} ; \ \left(\frac{\pi}{2} - \eta\right) \le \phi \le \frac{\pi}{2} \ \& \ \eta > 0$$

where T = net strap tension load

R = half shroud radius

η = 1/2 of the angle subtended by the circumferential wrap of the net around the half shroud

ϕ = angle between the split line and the section at which the moment is being calculated.

If it is assumed that the net strap load is distributed as a sine function with the maximum load occurring at the half shroud keel as shown in figure 13, the ring segment circumferential bending moment is given by,

$$M_\phi = \frac{TR}{2} \sin\eta \left[\cos\phi \ (2 - \cos\phi\ ) - 1\right] \quad (25)$$

$$0 \le \phi \le \left(\frac{\pi}{2} - \eta\right) \ \& \ \eta > 0$$

and

$$M_\phi = TR \left\{ \frac{\sin\eta}{2} \left[\cos\phi \ (2 - \cos\phi\ ) - 1\right] + \right.$$

$$\left. \frac{\sin\eta}{\eta + \sin\eta\cos\eta} \left[\left(\frac{\pi}{2} - \phi - \eta\right) \cos\phi - \sin\eta\cos(\eta + \phi)\right] \right.$$

$$\left(\frac{\pi}{2} - \eta\right) \le \phi \le \frac{\pi}{2} \ \& \ \eta > 0 \quad (26)$$

The maximum pressure on a single CSS corrugation is given by

$$P_{max} = \frac{4.32}{w} q_{max} = \frac{4.32}{w} \frac{2 \sin \eta}{\eta + \sin \eta \cos \eta} \frac{T}{R} \quad (27)$$

where w is the net strap width and T, R and η are the same as in equations 23 through 26. Equation 27 assumes a sine net strap load distribution with the maximum load occurring at the shroud keel as before. The constant 4.32 is based on the CSS corrugation cross section geometry

RESULTS AND DISCUSSION

Figure 14 is a graph of the CSS non-domed shell half rotation rate versus time for this analysis and one performed by Lockheed Missile and Space Company (LMSC). It can be seen that the analyses agree well if the Case I or early off condition is assumed. This analysis results in a constant angular velocity after hinge release of 53.8 degrees per second (.94 rad/sec) while the LMSC rate is 54.5 degrees per second (.95 rad/sec). If the Case II or late off condition is assumed, the constant angular rate at hinge release increases to 62.9 degrees per second (1.098 rad/sec).

Figure 15 shows shell half rotation angle from the vertical as a function of time for the two analyses. Again it can be seen that the analyses agree well up to the point of hinge release. For early off conditions (case I), this analysis results in a release angle of 60.8 degrees (1.06 rad) while the LMSC analysis gives 62.0 degrees (1.08 rad). Late off conditions (Case II) result in a release angle of 72.0 degrees (1.255 rad).

In order to evaluate the integrity of the catch net system prior to the actual CSS test and to observe the hinge separation, a simulated jettison into the catch net was performed using a full scale model of the half shroud. Although the model half shroud was a truss type structure covered with commercial grade corrugated skin, its size, weight, and center of gravity nearly matched that of the CSS non-domed half. High speed movie camera equipment focused on the model hinge indicated that the hinge release corresponded more nearly to the late off condition.

Figure 16 is a graph of half shroud angular velocity versus time for the early off case. The 1500 lbf (6675 newtons) brake cable tension and 8.4 deg (.1466 rad) net angle are the values selected during the original design of the catch net system. The time scale starts at 2.80 seconds after the initial shroud separation. This is an arbitrarily selected time which is after hinge separation and prior to net contact. It can be seen that the half shroud angular velocity is constant at 54 degrees per second (.941 rad/sec) until net contact at 2.96 seconds when the angular velocity decreases to 21 degrees per second (.366 rad/sec). Shroud angular velocity becomes zero at 3.28 seconds and then oscillates about zero. Continuous oscillation occurs because damping was neglected in the analysis.

Figure 17 shows the angular position of the half shroud as a function of time for the early off case. At the net contact time of 2.96 seconds obtained from the previous figure, the half shroud angle is 81.5 degrees (1.42 rad) from the vertical (8.5 degrees (.148 rad) from the horizontal). The design angle for the full jettison catch net is 8.4 degrees (.147 rad) from the horizontal. Theoretically then the half shroud should contact the net along the full length of the half shroud which is favorable for load distribution.

Half shroud angular velocity as a function of time is shown in Figure 18 for the late off case. The angular velocity is constant at 63 degrees per second (1.1 rad/sec) after hinge separation and net contact occurs at 2.96 seconds as before. Opposite 2.96 seconds in Figure 19, which shows shroud angular position for the late off case, the half shroud angle at net contact is 84.4 degrees (1.47 rad) from the vertical (5.6 degrees (.098 rad) from the horizontal). This indicates that the half shroud will make initial contact with the net on the biconic or nose section. High speed movies of the full scale model shroud test, referred to earlier, indicated that initial contact was in the biconic section. Load cells installed on the brake cables and on selected net straps confirmed this observation.

Figure 20 shows the stations along the half shroud length at which the longitudinal bending moment was calculated. Figure 21 is a graph of longitudinal bending moment versus time for station 274 and the early off case. Positive bending moment signifies tension on the half shroud keel and negative bending moment signifies tension on the half shroud split line. Brake cable tension for all cases was 1500 pounds (6675N). The maximum positive bending moment of 410,000 inch pounds (4.64×10^4 N-m) occurs at station 274 and the maximum negative bending moment of -263,000 inch pounds (-2.97×10^4 N-m) occurs at station 250 as shown in Figure 22. The allowable longitudinal half shroud bending moment is 1.0×10^6 inch pounds (1.13×10^5 N-m) for the heated tests and 2.0×10^6 inch pounds (2.26×10^5 N-m) for the unheated tests (Reference: LMSC Interdepartmental Communication IDC-S/I-482, D. W. Grant to M. E. Avery dated 4 May 1972).

Figure 23 shows longitudinal bending moment as a function of time at station 274 for the late off case. The maximum positive bending moment of 1.04×10^6 inch pounds (1.175×10^5 N-m) occurs at station 274 and the maximum negative bending moment of -320,000 inch pounds (-3.62×10^4 N-m) occurs at stations 250 and 344 as shown in Figures 24 and 25 respectively. The maximum positive bending moment occurs at initial net contact for the late off case whereas it occurs approximately 0.2 seconds after initial net contact for the early off case and is less than half the magnitude (410,000 inch pounds (4.64×10^4 N-m) versus 1.0×10^6 inch pounds (1.175×10^5 N-m)). The relatively high value for the late off case can be attributed to the concentrated net loads imposed on the half shroud biconic section during initial net contact when the half shroud attitude and net angle differ by approximately 3 degrees (.0524 rad).

Two cases were analytically investigated in which the net angle was reduced from 8.4 degrees (.147 rad) to 6.4 degrees (.112 rad) and to 4.4 degrees (.077 rad). This was theoretically accomplished by rotating the net frame about the middle brake position so that the hinge end of the net was raised and the nose end lowered. Physical constraints within the catch net system required that the middle brake position be selected as the pivot point. Figure 26 shows the half shroud initial contact angle for the net design angle of 8.4 degrees (.147 rad) and the two alternate angles of 6.4 degrees (.112 rad) and 4.4 degrees (.077 rad). It can be seen that the half shroud contacts the net along the full length of the half shroud for the early off case and a net angle of 8.4 degrees (1.47 rad). For the same net angle and the late off case, initial contact is made on the half shroud biconic section. Reducing the net angle to 6.4 degrees (.112 rad) results in the half shroud hinge end making initial contact for the early off case and essentially full length contact for the late off case. Further net angle reduction to 4.4 degrees (.077 rad) results in half shroud hinge end initial contact for both cases.

The maximum positive and negative longitudinal bending moments for the above cases are summarized in Table I. The maximum positive bending moment for the late off case decreases with decreasing net angle and the magnitude of the negative bending moment increases but to a lesser degree. For the early off case, the maximum positive bending moment and the negative bending moment absolute values increase with decreasing net angle but remain well below the allowable. Based on these three cases, the net angle should be such that initial net contact on the biconic section of the shroud is avoided. An angle of 5.5 to 6.5 degrees (.096 to .113 rad) is desirable to keep bending moments below the allowable for both early off and late off conditions and a brake cable tension of 1500 pounds (6676N).

Figure 27 shows the theoretical maximum positive and negative ring segment circumferential bending moments as a function of net strap wrap half angle. Positive moment due to strap load decreases the half shroud radius of curvature and negative moment due to deceleration force increases the radius of curvature. The uniform distribution curve represents values obtained from equations 23 and 24 and the sine distribution curve represents values obtained from equations 25 and 26. The dimensionless ordinate quantity is the maximum positive or negative moment per pound of strap tension force per inch of radius obtained when varying the angle ϕ for a particular value of the wrap half angle η. For wrap half angles between 10 and 50 degrees (.1745 and .862 rad) the moment is negative along the entire half shroud circumference so that the maximum moment is negative. Between 50 and 90 degrees (.862 and 1.57 rad) there is a maximum positive moment and a maximum negative moment that exist along the circumference. For half wrap angles greater than 65 degrees (1.13 rad), the maximum negative moment is small when compared to the maximum positive moment and goes to zero at a wrap half angle of 90 degrees (1.57 rad).

The maximum allowable negative circumferential bending moment for any half shroud ring segment is 3255 inch-lbs (367 N-m). The maximum allowable positive circumferential bending moment for any half shroud ring segment is 5230 inch-lbs. (591 N-m). (Reference: LMSC Interdepartmental Communication, R. G. Pinkert to M. E. Avery, dated 10 January 1973.) Using these values and equations 23 through 26, the maximum allowable strap tension forces that can be applied to a ring segment are calculated and plotted as a function of half wrap angle in Figures 28 through 30. Figure 28 shows the maximum allowable strap tension forces for the cylindrical section of the half shroud. Maximum allowable strap forces for the uniform and sine strap load distribution are shown. The angle range of 45 to 65 degrees (.785 to 1.132 radians) represents the range of net wrap half angles from the time the half shroud makes initial contact with the net to its final rest position. This angle range is ideally located where the values of the maximum allowable strap loads are the greatest. The theoretical maximum strap tension loads experienced by the half shroud are also plotted for the early off and late off cases and two net attitude angles. All of these loads are below the allowable strap tension loads for both distributions.

Figure 29 shows the maximum allowable strap tension load in the vicinity of brake 4 which is located within the 15 degree (.262 radian) shroud cone section. The radius at this location is approximately 75 inches (1.93m). The same ring segment allowable bending moments are assumed to apply. Theoretical strap tension loads for brake position 4 and the net wrap half angle range are shown. It can be seen that the strap tension loads are slightly lower for the smaller net attitude angle of 6.4 degrees (.112 radians).

Figure 30 is a graph of the maximum allowable strap tension load in the vicinity of brake 5 which is closest to the half shroud nose end. The radius is approximately 42 inches (1.068m) and the same ring segment allowable bending moments are assumed to apply. The theoretical maximum strap tension load for the late off case is approximately 100 lbs (447N) higher than the sine distribution allowable. Lowering the net angle to 6.4 degrees (.112 radians) reduces the load so that it is below the allowable for both distribution cases.

Maximum corrugation pressure versus net strap tension for two half wrap angles is shown in Figure 32. The maximum predicted strap tension load on the CSS cylindrical section is 365 pounds (1625N) for the late off case, 1500 pounds (6675N) brake cable tension and a 8.4 degree (.147 rad) net angle. For the early off case and the same cable tension and net angle, the maximum strap tension load is 510 pounds (2270N). Only the cylindrical section is of concern because it is the only part that is covered with corrugated skin. The biconic section is smooth skinned. Strap tension loads of 365 pounds (1625N) and 510 pounds (2270N) result in corrugation pressures of 24 psi (1.655×10^5 N/m^2) and 33 psi (2.28×10^5 N/m^2) respectively for a half wrap angle of 90 degrees (1.57 rad). Actually the maximum possible half wrap angle in the cylindrical section is about 70 degrees (1.22 rad) due to the physical dimensions and arrangement of the catch net system. It can be seen that even if the strap tension equaled the brake cable tension of 1500 pounds (6675N), the 90 degree (1.57 rad) half wrap angle corrugation pressure of 98 psi (6.75×10^5 N/m^2) is well below the allowable pressure of 232 psi (1.60×10^6 N/m^2).

CONCLUDING REMARKS

The CSS rigid body dynamic analysis was performed to predict possible problem areas in the SPF catch net system with particular attention to the longitudinal bending moment loads imposed on the CSS by the catch net. The conclusions drawn from the analysis are:

1. Hinge release point is an important factor in determining the attitude of the half shroud at net contact.

2. Initial net contact on the biconic section only should be avoided to keep longitudinal and circumferential bending moments within allowable limits.

3. Adjusting the net angle to accommodate full length contact for the late off condition produces acceptable longitudinal bending moments for both hinge release cases.

4. Corrugation pressures are well below the allowable pressure even for an extreme half wrap angle of 90 degrees (1.57 rad).

APPENDIX A

SYMBOL LIST

b_i	Y axis intercept
C_1	Constant horizontal translational velocity of the half shroud following hinge separation and prior to net contact
C_2	Constant angular velocity of the half shroud following hinge separation and prior to net contact
CL	Brake cable length between the brake and net frame
F_1	Breakaway spring force
F_2	Jettison spring force
F_B	Constant preset cable tension required to overcome brake friction
F_{ci}	Brake cable force at station i
F_i	Vertical net force at station i
F_j	Vertical net force at stations forward or aft of section m-m
F_{si}	Total net strap tension force at station i
g	Acceleration due to gravity
I_{cg}	Mass moment of inertia of the total mass forward of section m-m
I^s_{cg}	Half shroud mass moment of inertia about its center of gravity
I_F	Frame mass moment of inertia about its center of gravity
I^s_o	Mass moment of inertia of the half shroud about the hinge point
1_1	Distance from the half shroud hinge point to breakaway spring location
1_2	Distance from the half shroud hinge point to jettison spring location

l_3	Distance from the half shroud hinge point to half shroud center of gravity
m	Total mass forward or aft of section m-m
m_F	Frame mass
M_{m-m}	Longitudinal bending moment at section m-m
m_s	Mass of the half shroud
M_ϕ	Circumferential bending moment at ϕ
n_i	Shroud profile line slope
NL	Net length between the net frame and the point of tangency of a line drawn from the brake centerline to the half shroud circumference
P_{max}	Maximum pressure on a single CSS corrugation
q	Load per inch on shroud circumference due to net strap
R	Shroud radius
T	Net strap tension load
TL	Total shaped length of thenet and brake cable
w	net strap width
W_i^F	Frame weight at brake station i
W_s	Weight of the half shroud
W_{TF}	Total frame weight
X_{cg}	Distance from the half shroud center of gravity to the center of gravity of the total mass forward or aft of section m-m
X_{cg}^s	Horizontal distance from the fixed hinge point to the half shroud center of gravity

X_i^F	Distance from the frame center of gravity to brake cable i
X_i^s	Distance from the half shroud center of gravity to brake cable station i
X_j	Distance from the half shroud center of gravity to brake stations forward or aft of section m-m
X_m	Distance from the half shroud center of gravity to section m-m
YB	Distance from brake centerline to split line of half shroud when half shroud is in the net
Y_{cg}^F	Vertical distance from the fixed hinge horizontal plane to the frame center of gravity
Y_{cg}^s	Vertical distance from the fixed hinge horizontal plane to the half shroud center of gravity
ZB	Horizontal distance from the brake centerline to the half shroud centerline when the half shroud is in the net

GREEK LETTERS

η	Brake cable angle with the horizontal and the net wrap half angle
Θ	Angle measured about the hinge point from the horizontal plane to the half shroud base plane or the angle from the vertical to the half shroud keel line (Figures 7 and 8)
Θ_1	Angle between the half shroud base plane and a line drawn from the half shroud hinge point to the breakaway spring location (F_1)
Θ_3	Angle between the half shroud base plane and a line drawn from the hinge point to the half shroud center of gravity
Θ_F	Angle of the frame with the horizontal
ϕ	Angle between the split line and the section at which the circumferential bending moment is calculated

TABLE I

SHROUD MAXIMUM POSITIVE AND NEGATIVE LONGITUDINAL BENDING MOMENT FOR VARIOUS NET ANGLES

NET ANGLE		EARLY OFF				LATE OFF			
		BENDING MOMENT		STATION		BENDING MOMENT		STATION	
DEG.	RAD.	INCH LBF	NEWTON METERS	INCHES	METERS	INCH LBF.	NEWTON METERS	INCHES	METERS
8.4	.1466	4.10×10^5	4.63×10^4	274	6.96	10.4×10^5	11.75×10^4	274	6.96
		-2.63	-2.97	250	6.35	-3.20	-3.62	250 344	6.35 8.74
6.4	.1119	5.40	6.10	274	6.96	6.00	6.78	274	6.96
		-4.50	-5.08	250	6.35	-3.40	-3.84	344	8.74
4.4	.0768	6.07	6.86	274	6.96	5.00	5.65	469	11.9
		-4.52	-5.11	344	8.74	-4.70	-5.31	250 344	6.35 8.74

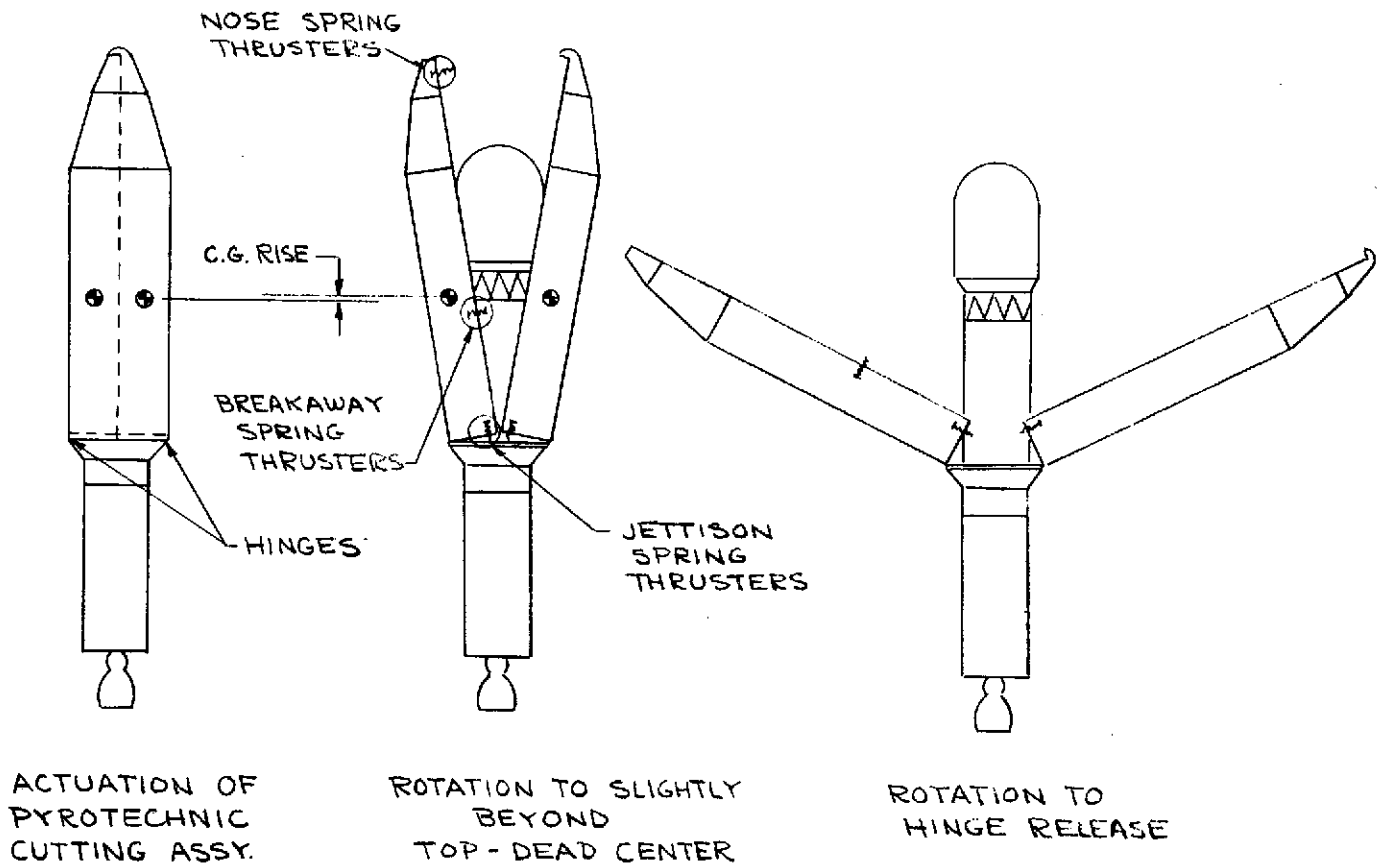

FIG. 1 - JETTISON SEQUENCE

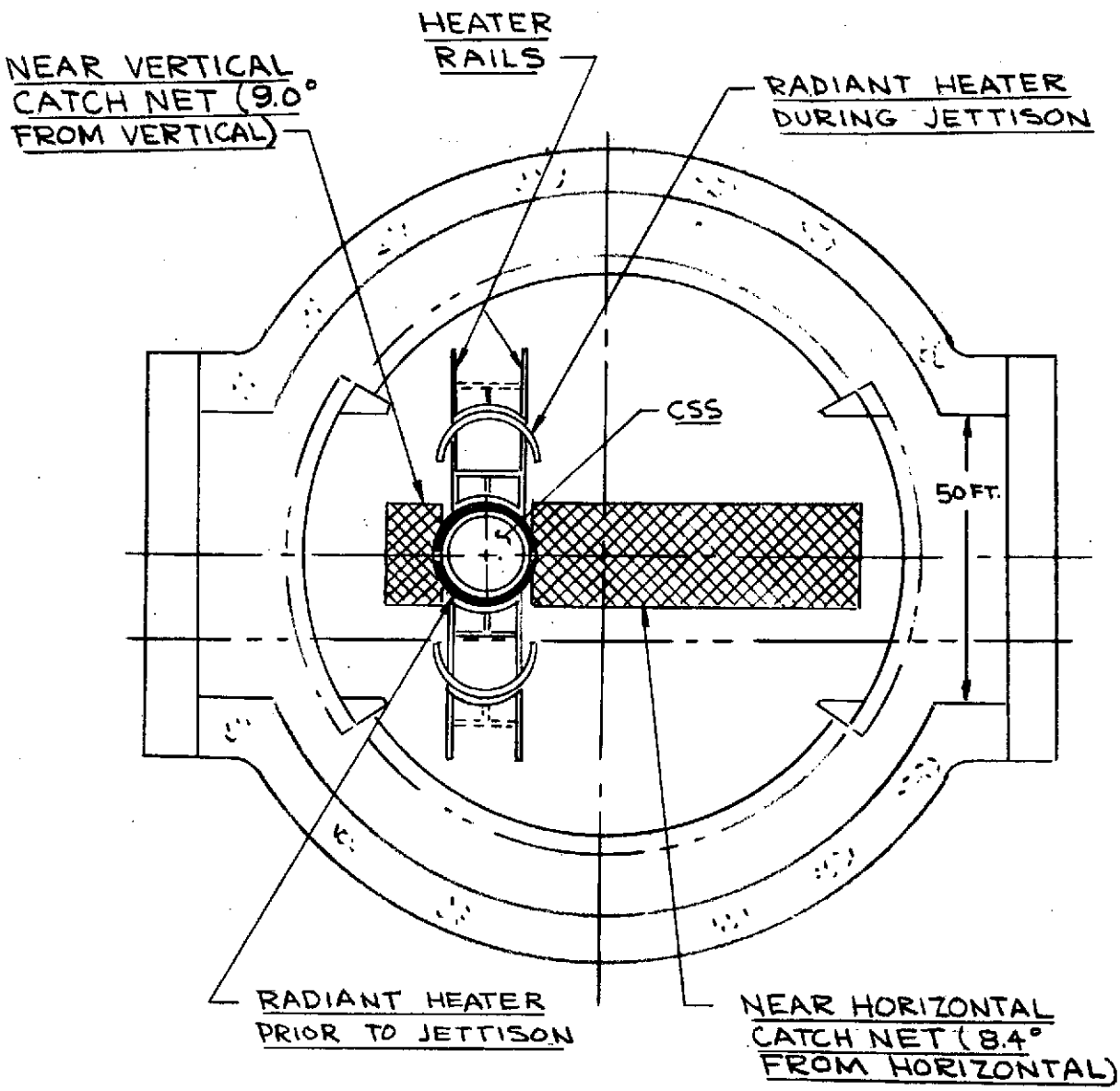

FIG. 2 - PLAN VIEW OF TEST HARDWARE IN SPACE POWER FACILITY

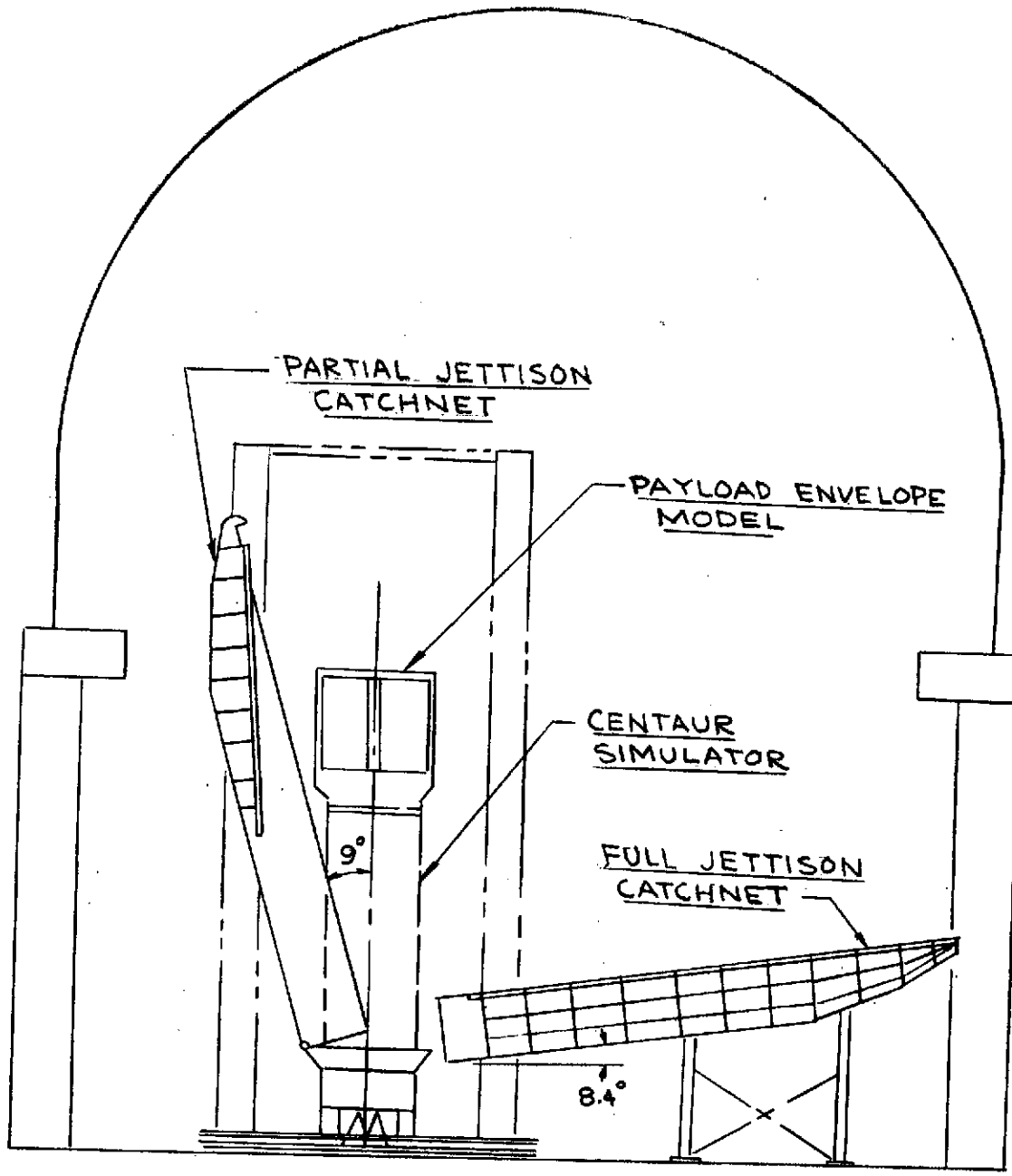

FIG. 3 - ELEVATION VIEW OF TEST HARDWARE IN SPACE POWER FACILITY SHOWING SHROUD HALVES MAKING INITIAL NET CONTACT.

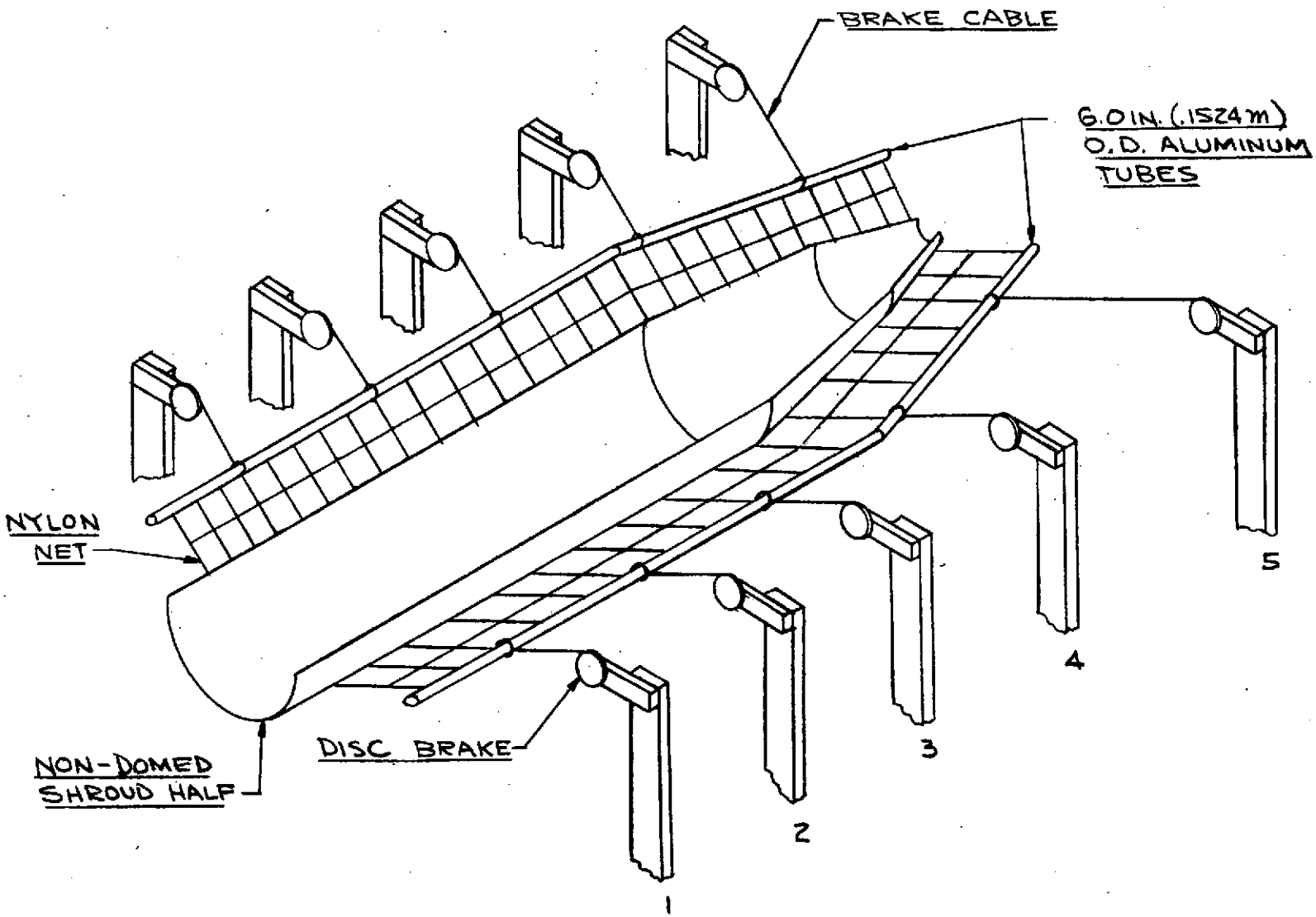

FIGURE 4 CSS FULL JETTISON CATCH NET SYSTEM

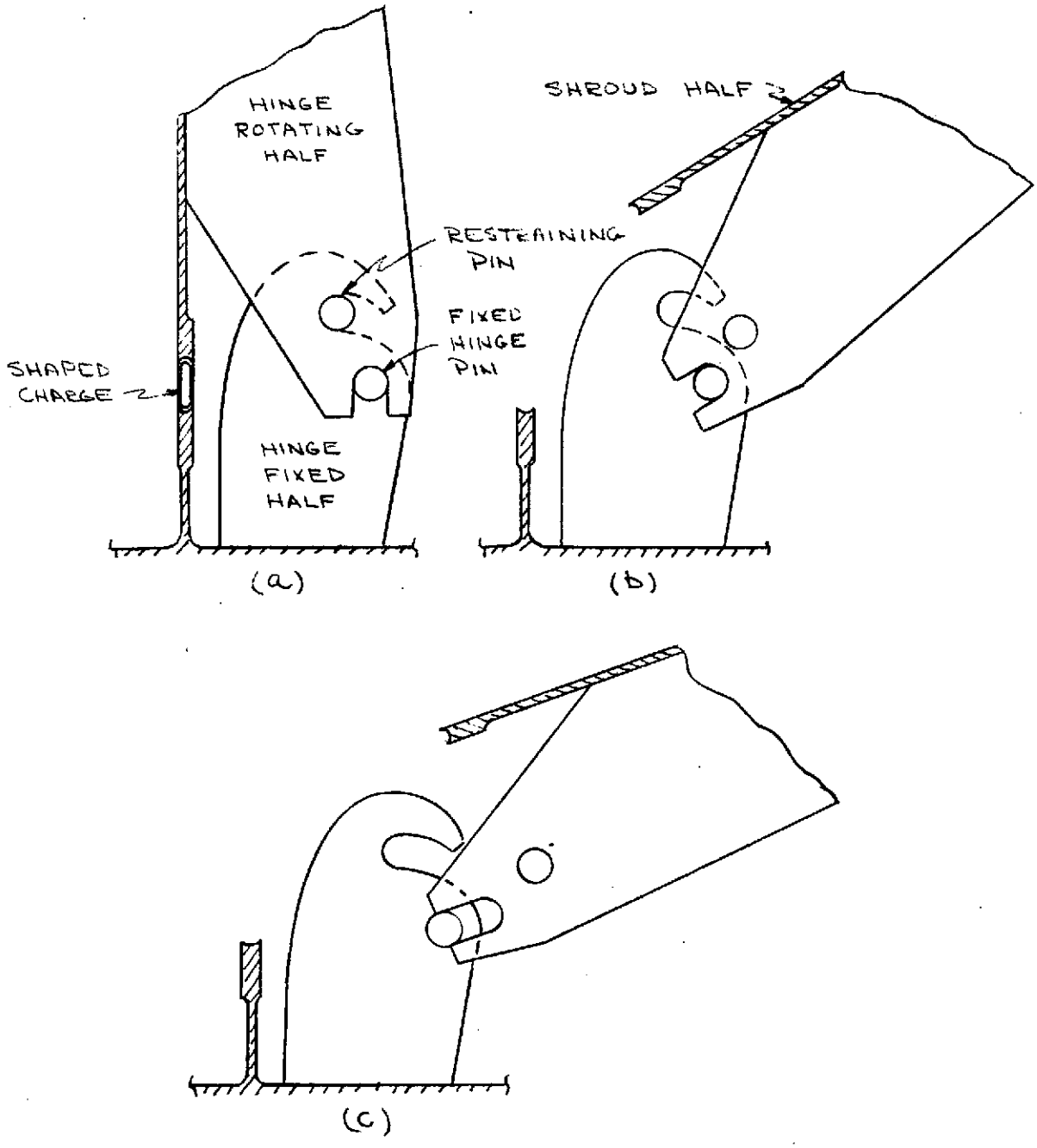

FIG 5 - HINGE SEPARATION

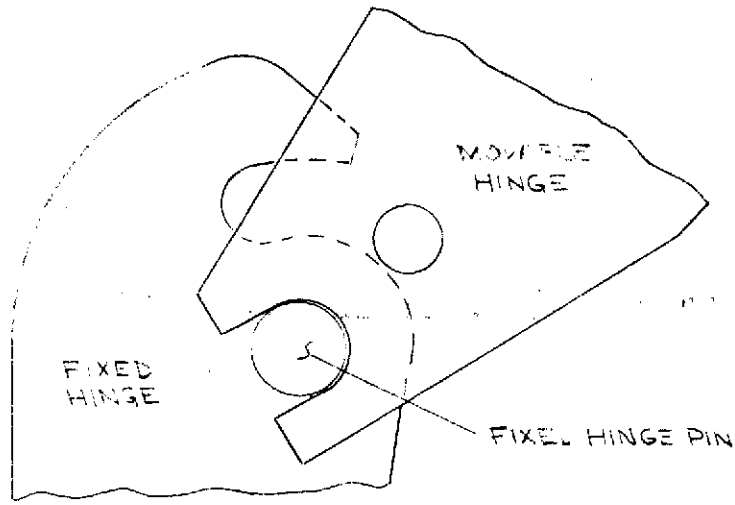

CASE I - HINGE RELEASE WHEN SLOT LIFTS OFF PIN

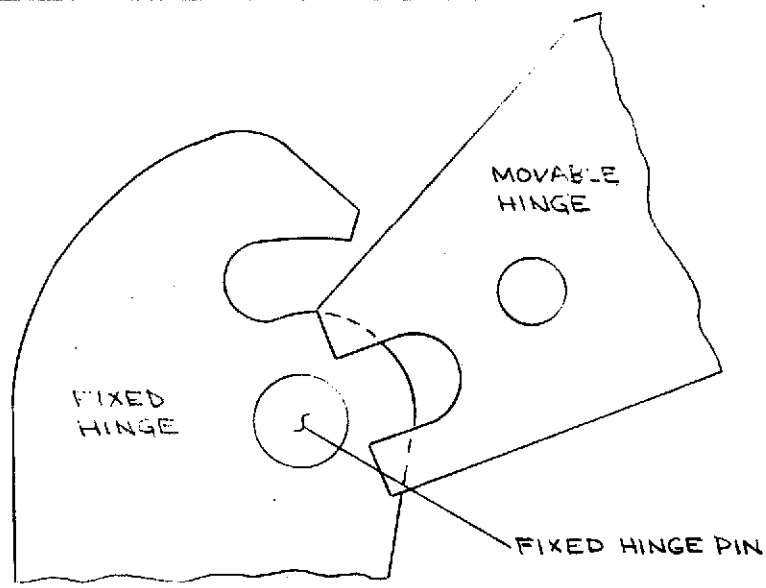

CASE II - HINGE RELEASE WHEN SLOT CLEARS PIN

FIGURE 6 - CSS THEORETICAL HINGE RELEASE POSITIONS

BY..... DATE..... SUBJECT..... SHEET NO..... OF .....

CHKD. BY ..... DATE..... JOB NO.....

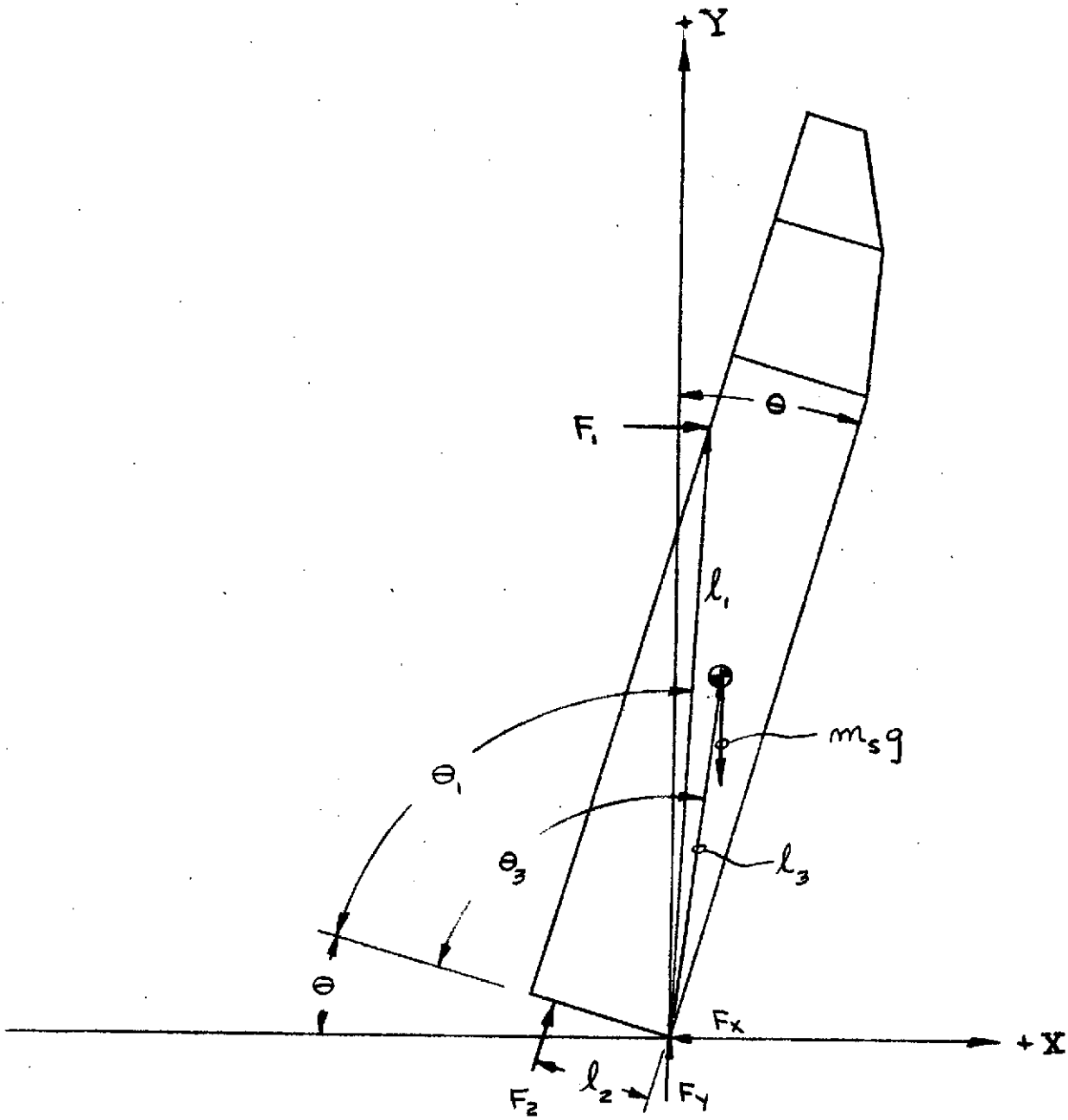

FIGURE 7 - FORCES ACTING ON CSS AT THE TIME OF INITIAL SEPARATION

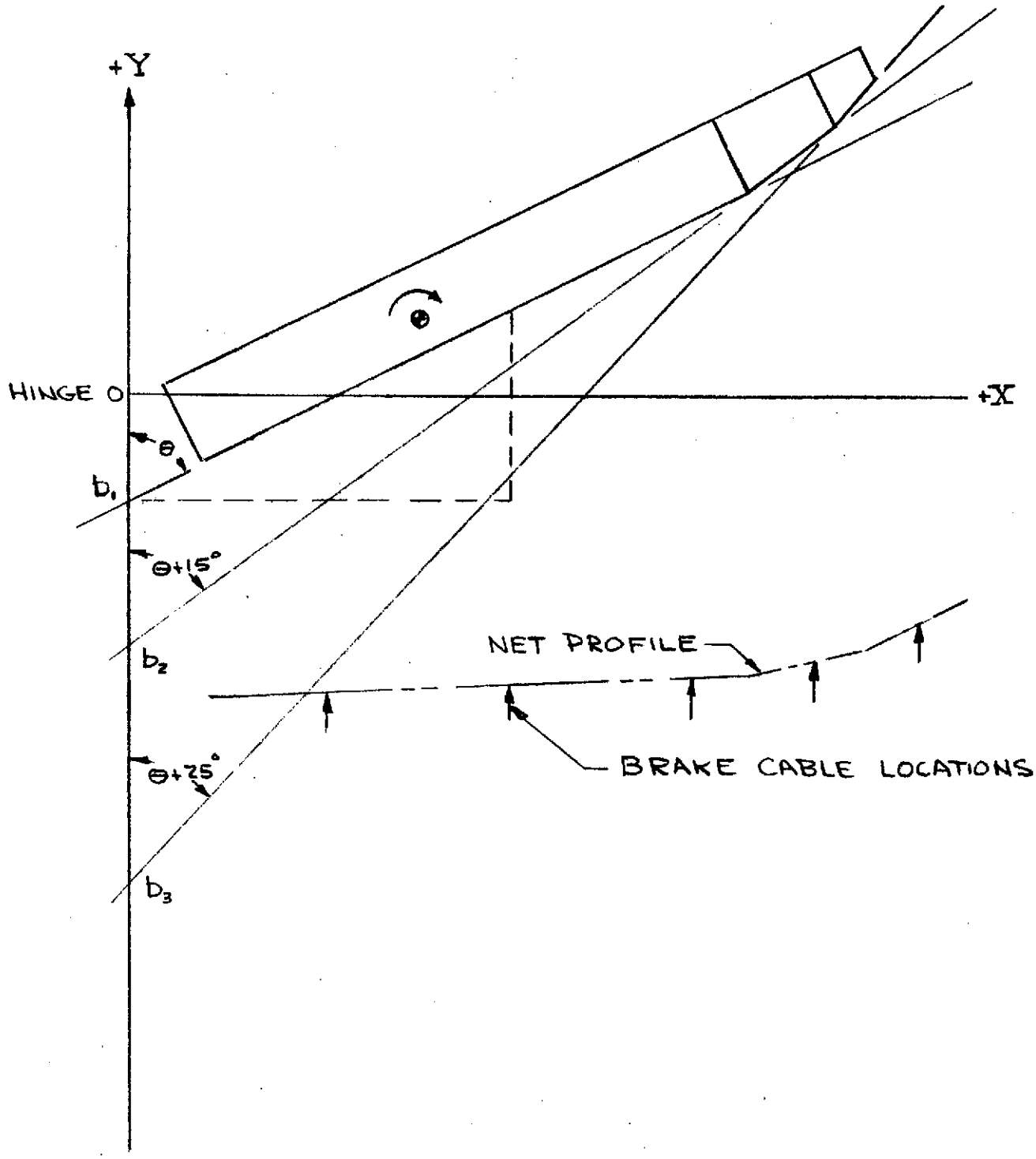

FIGURE 8 - LINES USED TO DEFINE THE HALF SHROUD PROFILE DURING FREE FALL

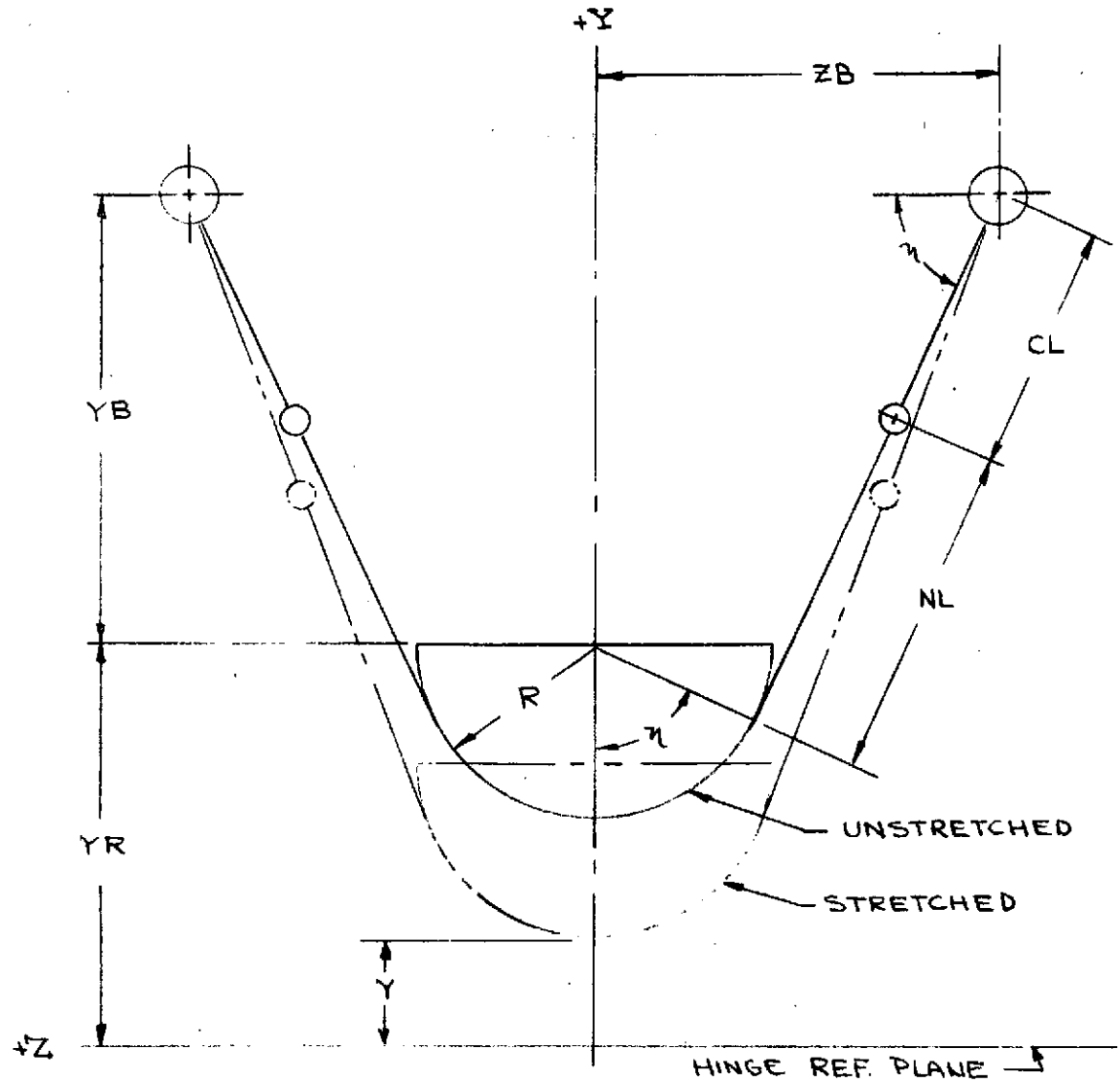

FIGURE 9 - TYPICAL BRAKE STATION CROSS SECTION SHOWING NET AND CABLE GEOMETRY

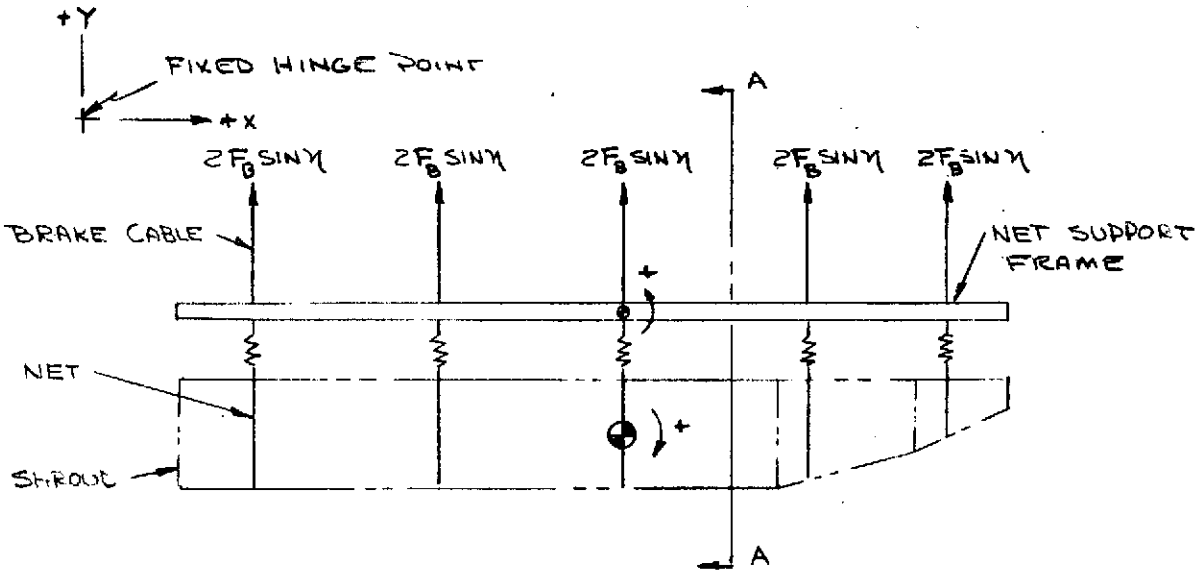

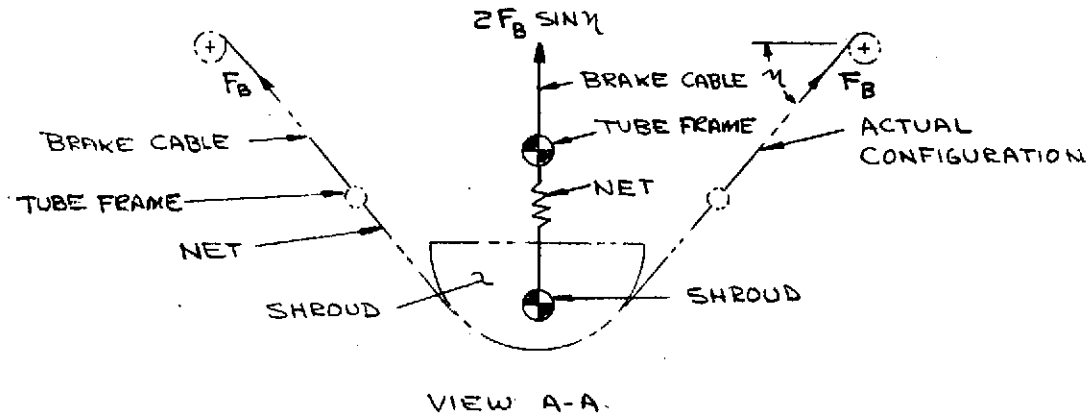

VIEW A-A

FIGURE 10 - CSS AND CATCHNET DYNAMIC MODEL

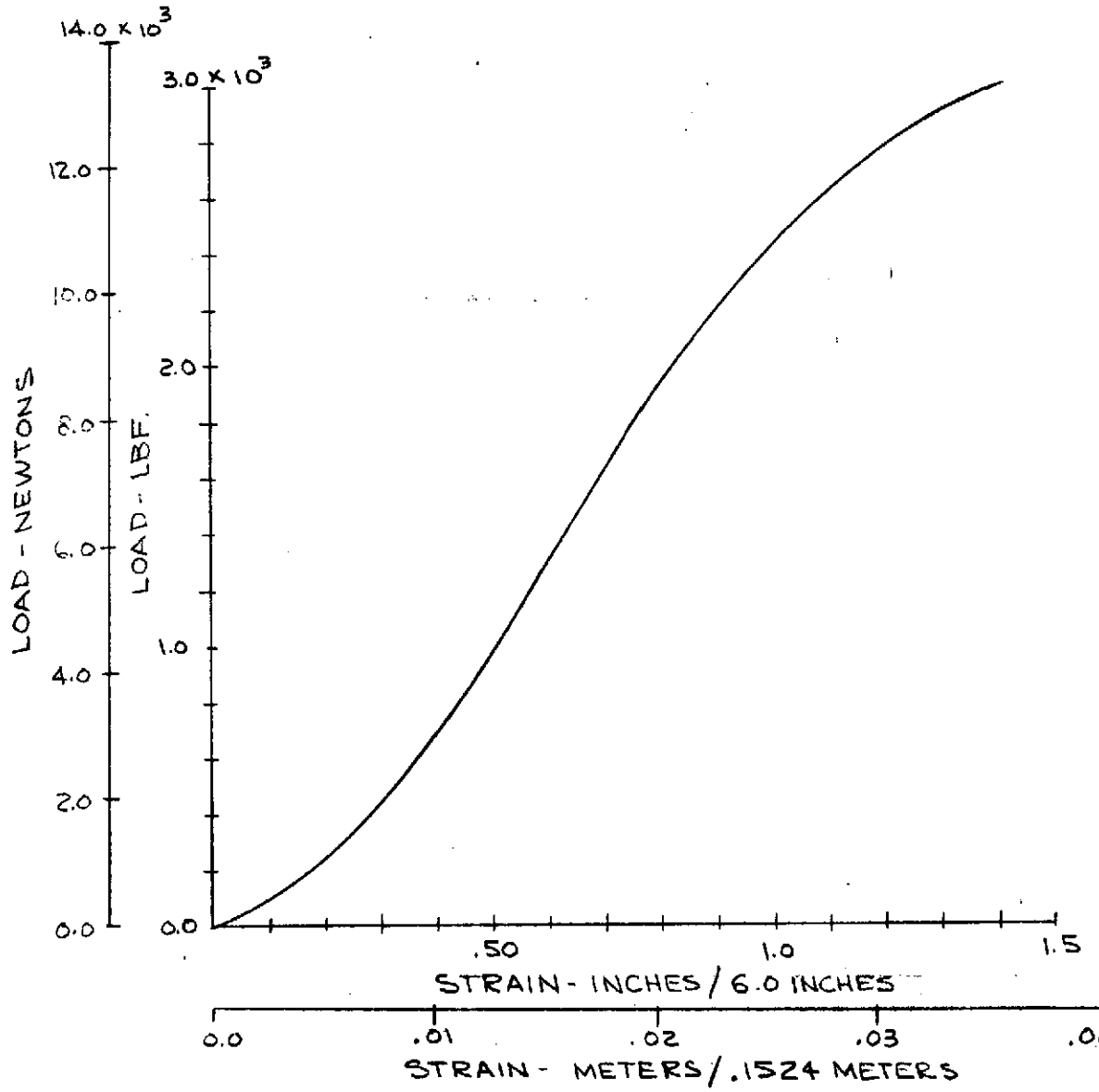

FIGURE 11 - LOAD VERSUS STRAIN CURVE FOR A SINGLE CATCHNET STRAP; 1.0 IN. (.0254m) WIDE x .12 IN. (.00305m) THICK NOMEX; 20 IN/MIN (.508 m/MIN) LOAD RATE

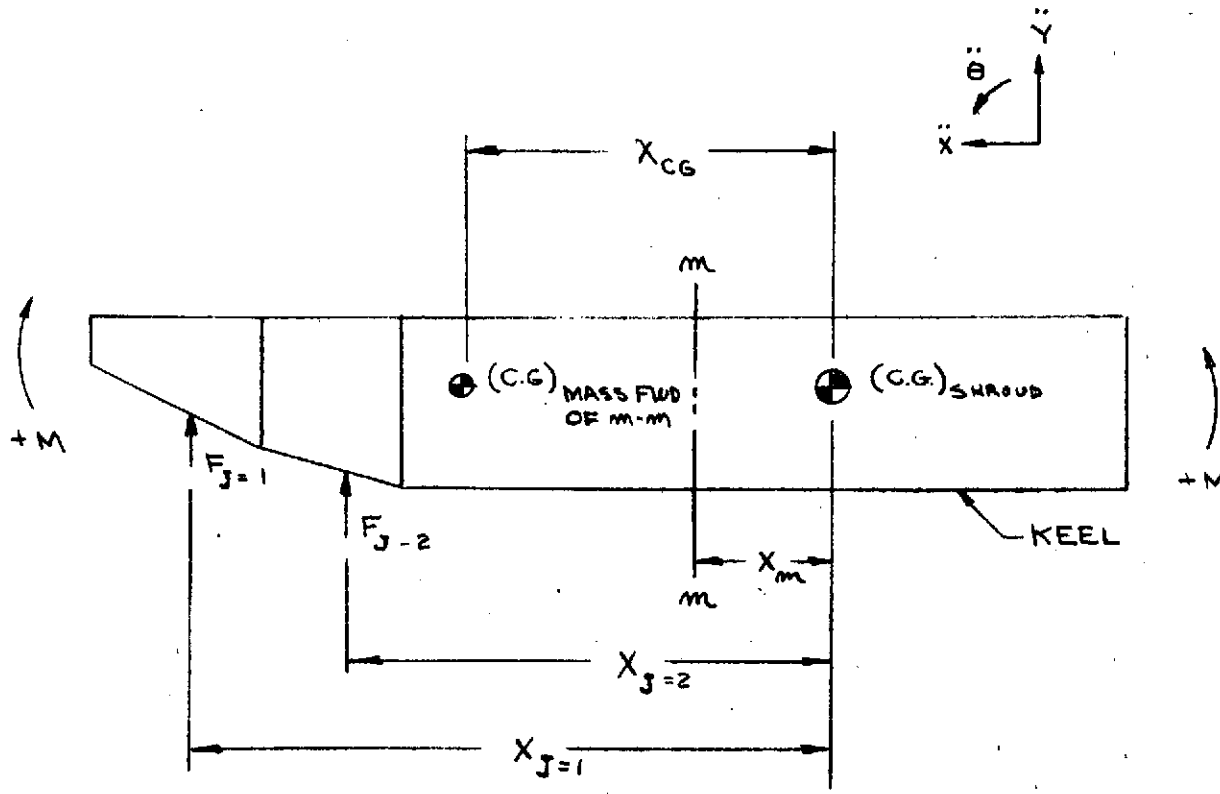

+ BENDING MOMENT = TENSION ON KEEL.

FIGURE 12 - LONGITUDINAL BENDING MOMENT FORCES AND MOMENT ARMS FOR A TYPICAL CROSS SECTION.

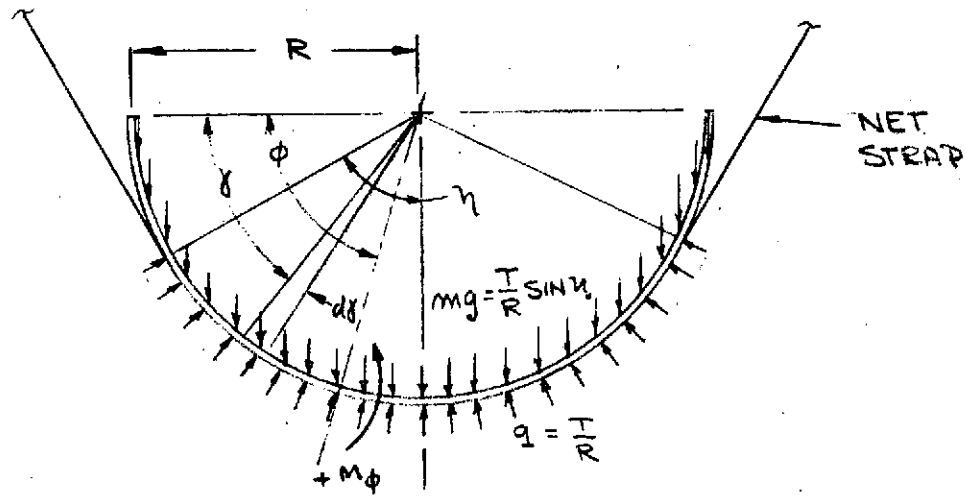

UNIFORM NET STRAP LOAD DISTRIBUTION

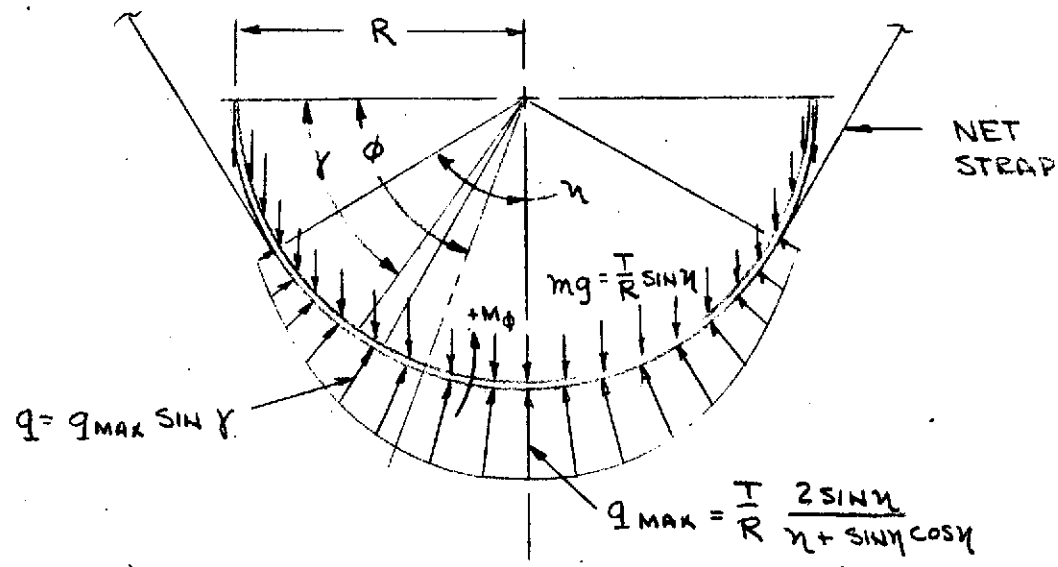

SINE FUNCTION NET STRAP LOAD DISTRIBUTION

FIG 13 - NET STRAP LOAD DISTRIBUTION

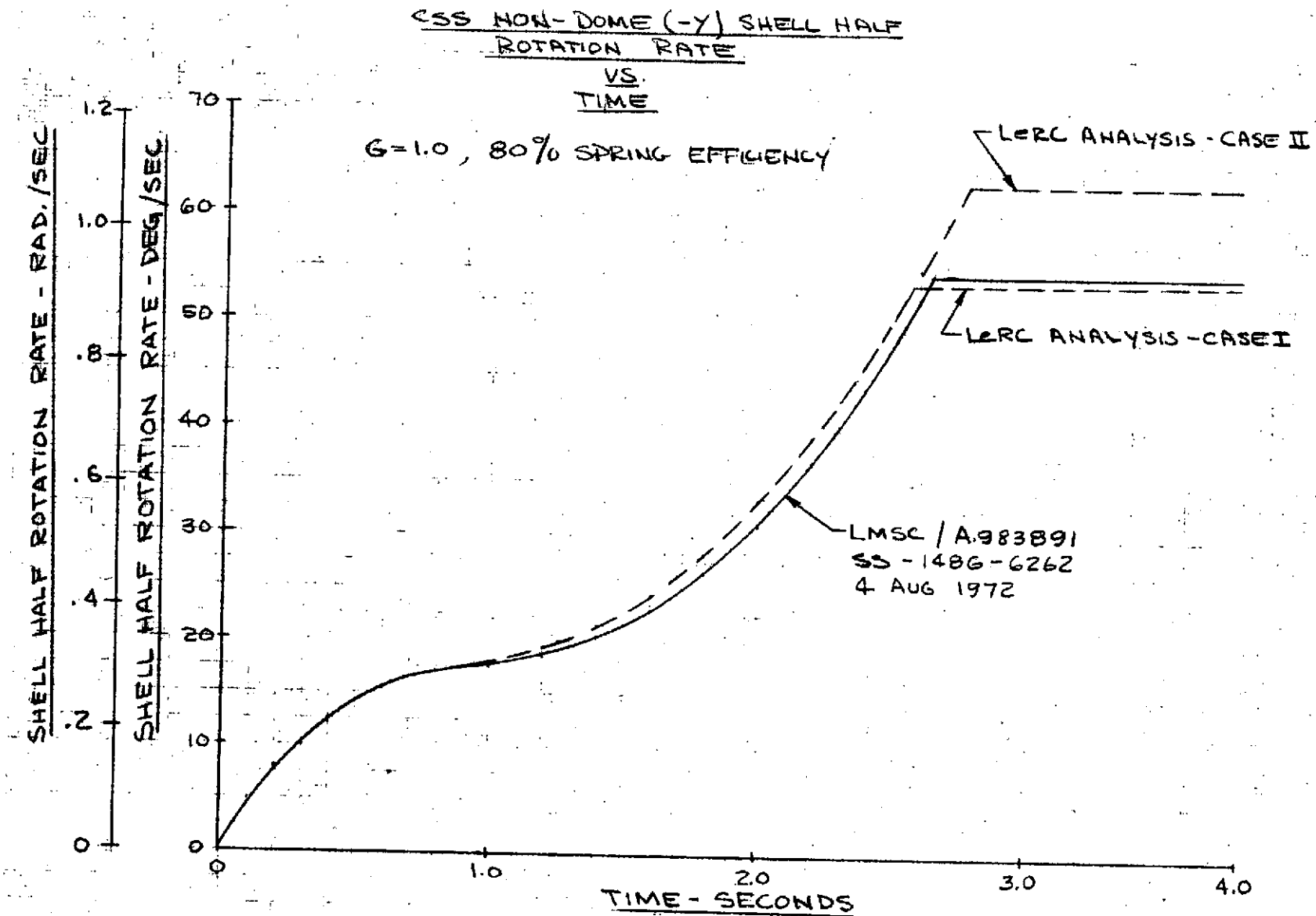

FIGURE 14- CSS NON-DOME SHELL HALF ROTATION RATE VS. TIME

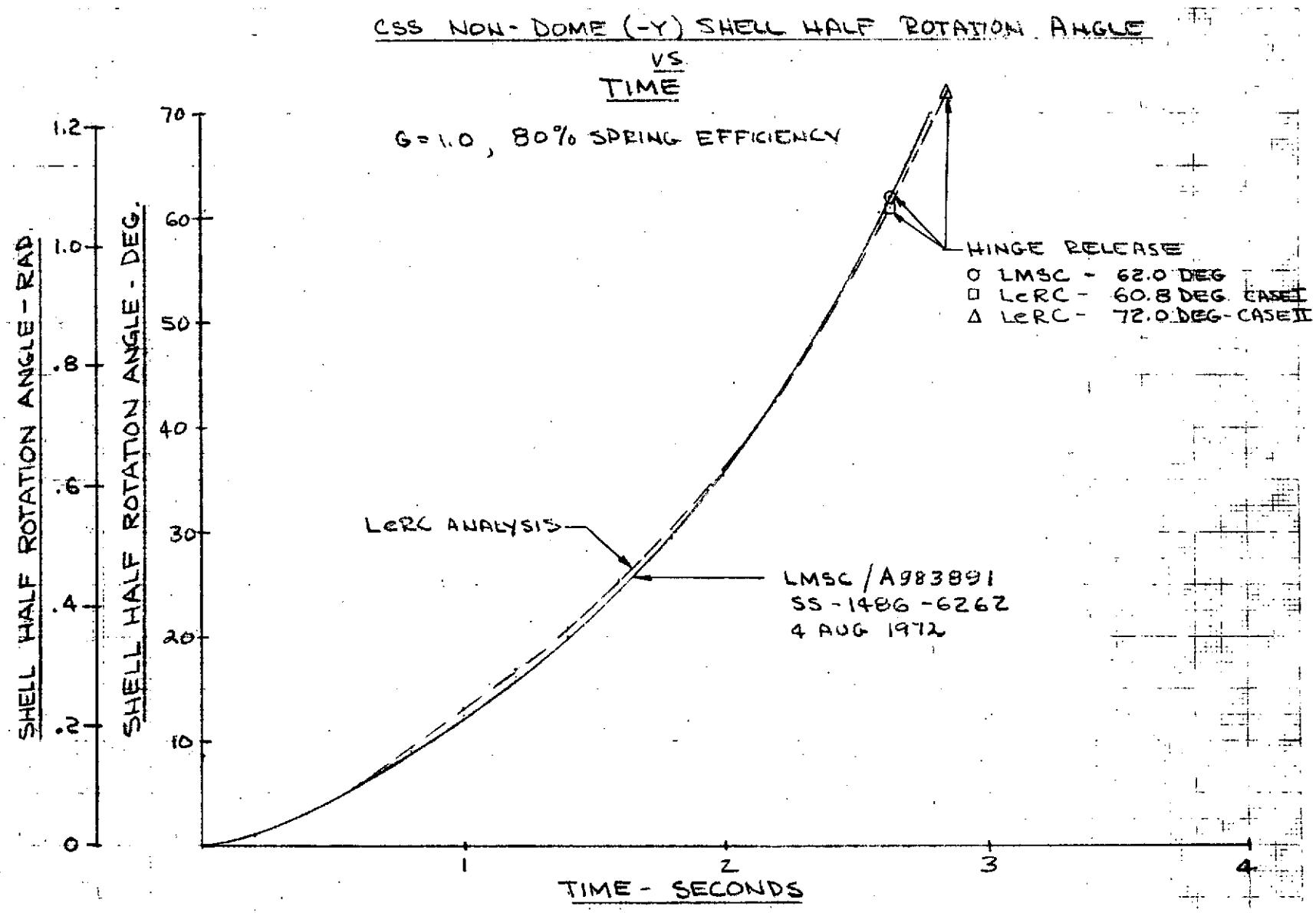

FIGURE 15 - CSS NON-DOME SHELL HALF ROTATION ANGLE VS. TIME

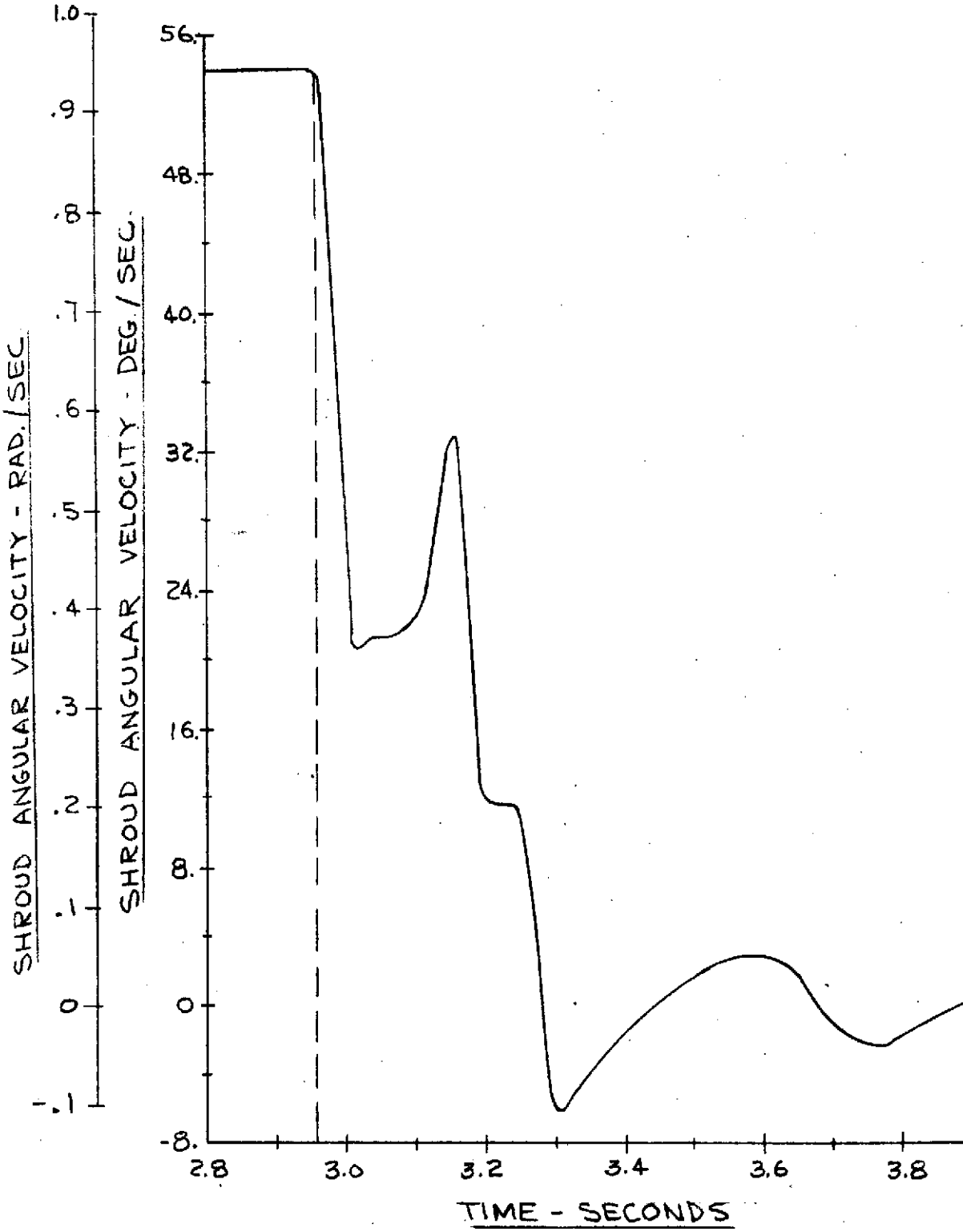

FIGURE 16 - SHROUD ANGULAR VELOCITY VS. TIME; EARLY OFF CASE; 1500 LBF (6675 NEWTONS) BRAKE CABLE TENSION; 8.4 DEG. (.1466 RAD) NET ANGLE.

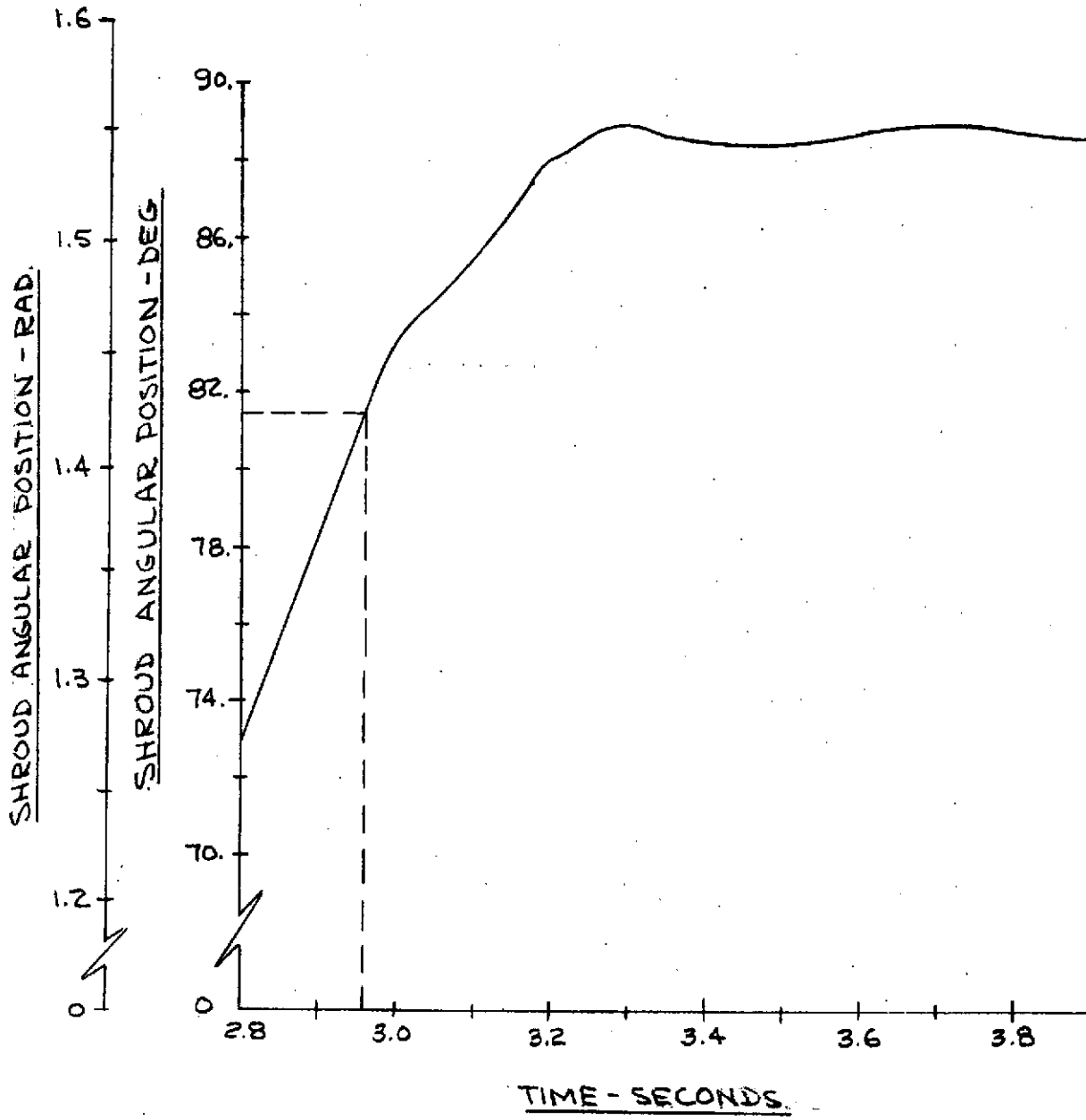

FIG. 17 - SHROUD ANGULAR POSITION VS TIME; EARLY OFF CASE; 1500 LBF. (6675 NEWTONS) BRAKE CABLE TENSION; 8.4 DEG (.1466 RAD.) NET ANGLE.

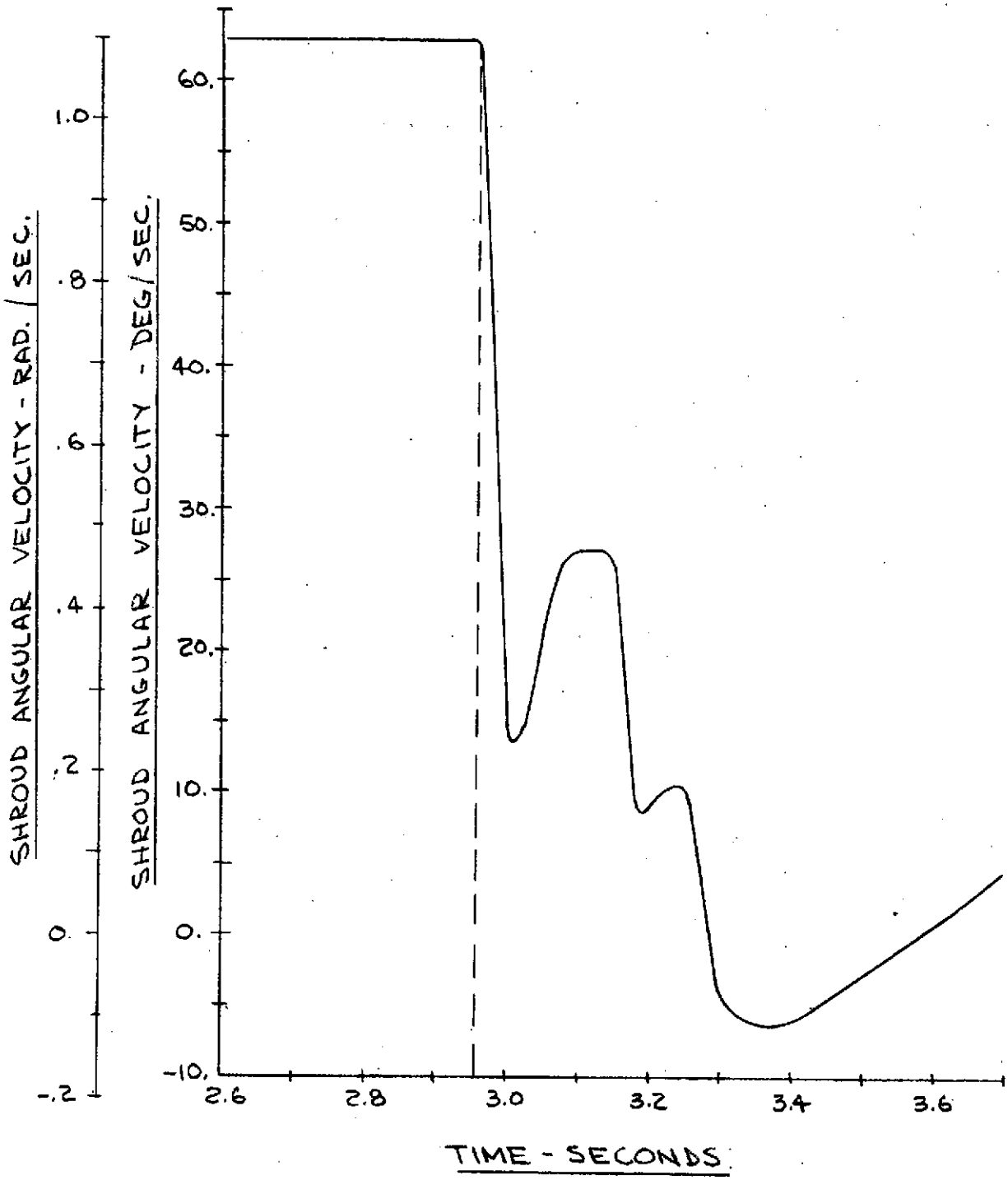

FIG. 18 - SHROUD ANGULAR VELOCITY VS. TIME; LATE OFF CASE; 1500 LBF (6675 NEWTONS) BRAKE CABLE TENSION; 8.4 DEG (.1466 RAD.) NET ANGLE

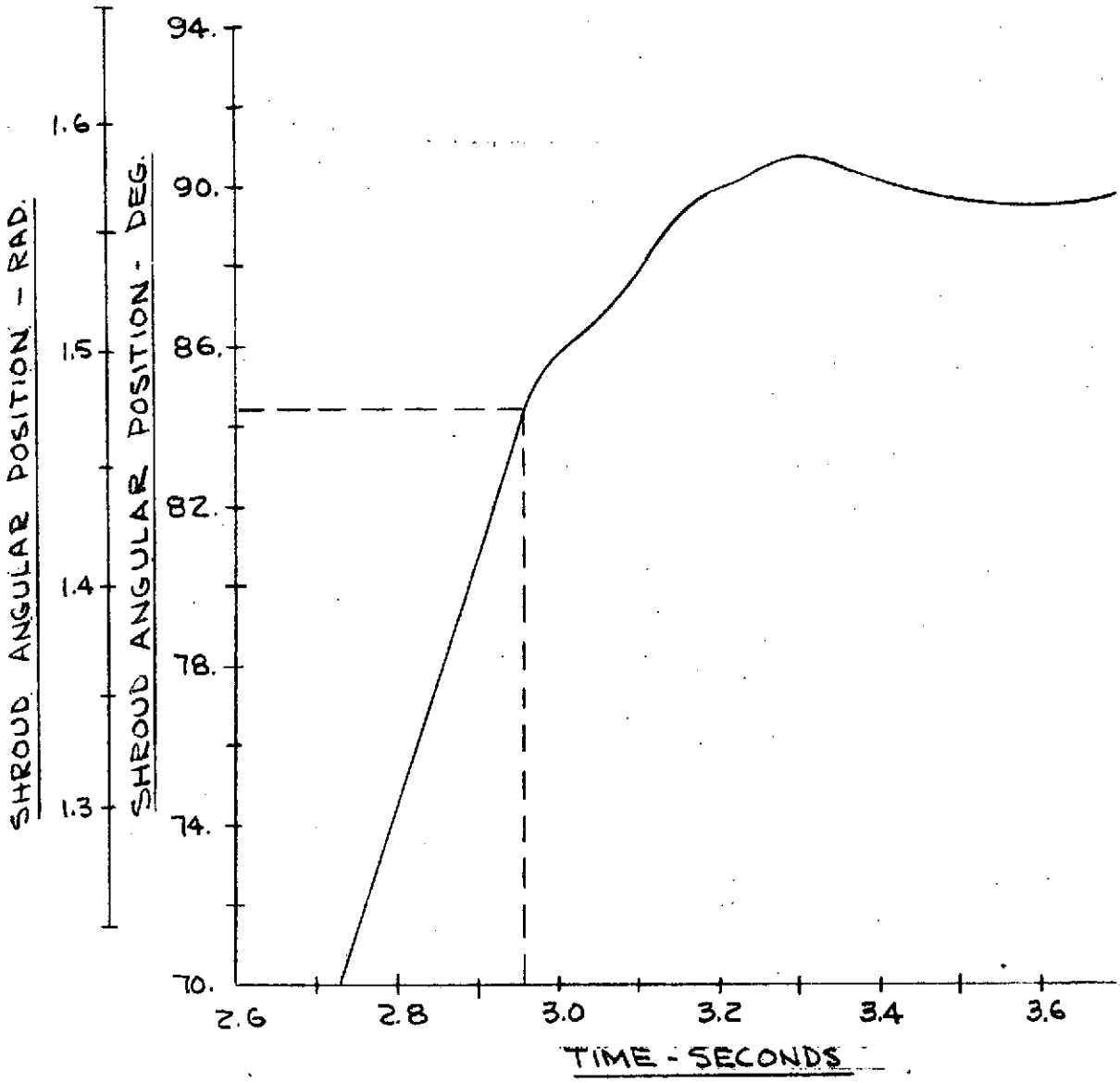

FIG 19- SHROUD ANGULAR POSITION VS. TIME; LATE OFF CASE; 1500 LBF (6675 NEWTONS) BRAKE CABLE TENSION; 8.4 DEG. (.1466 RAD.) NET ANGLE.

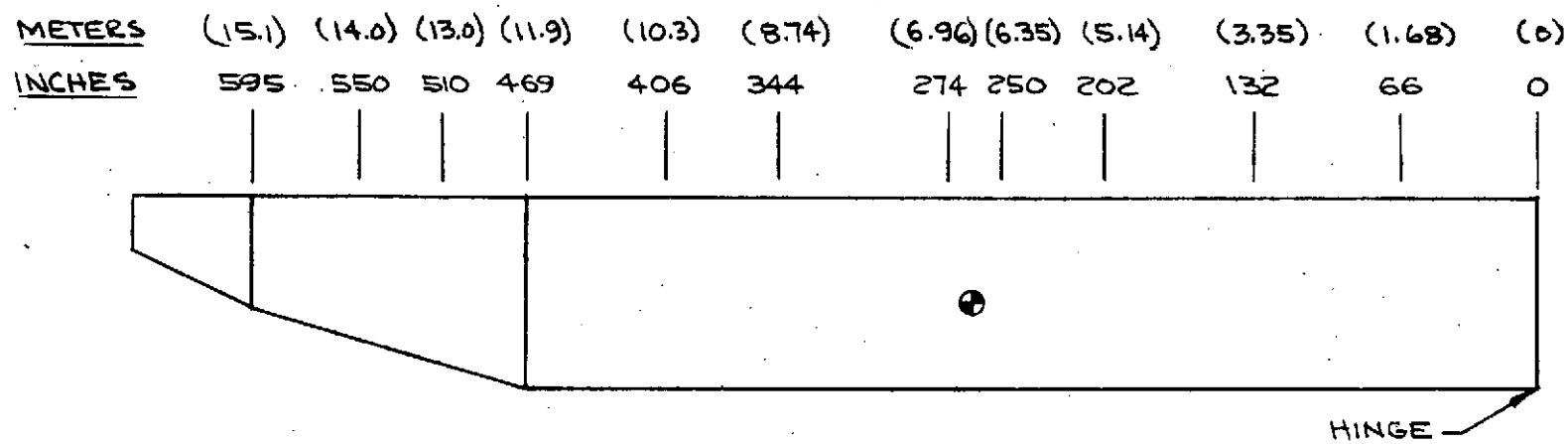

FIG. 20 STATIONS AT WHICH LONGITUDINAL BENDING MOMENT IS CALCULATED

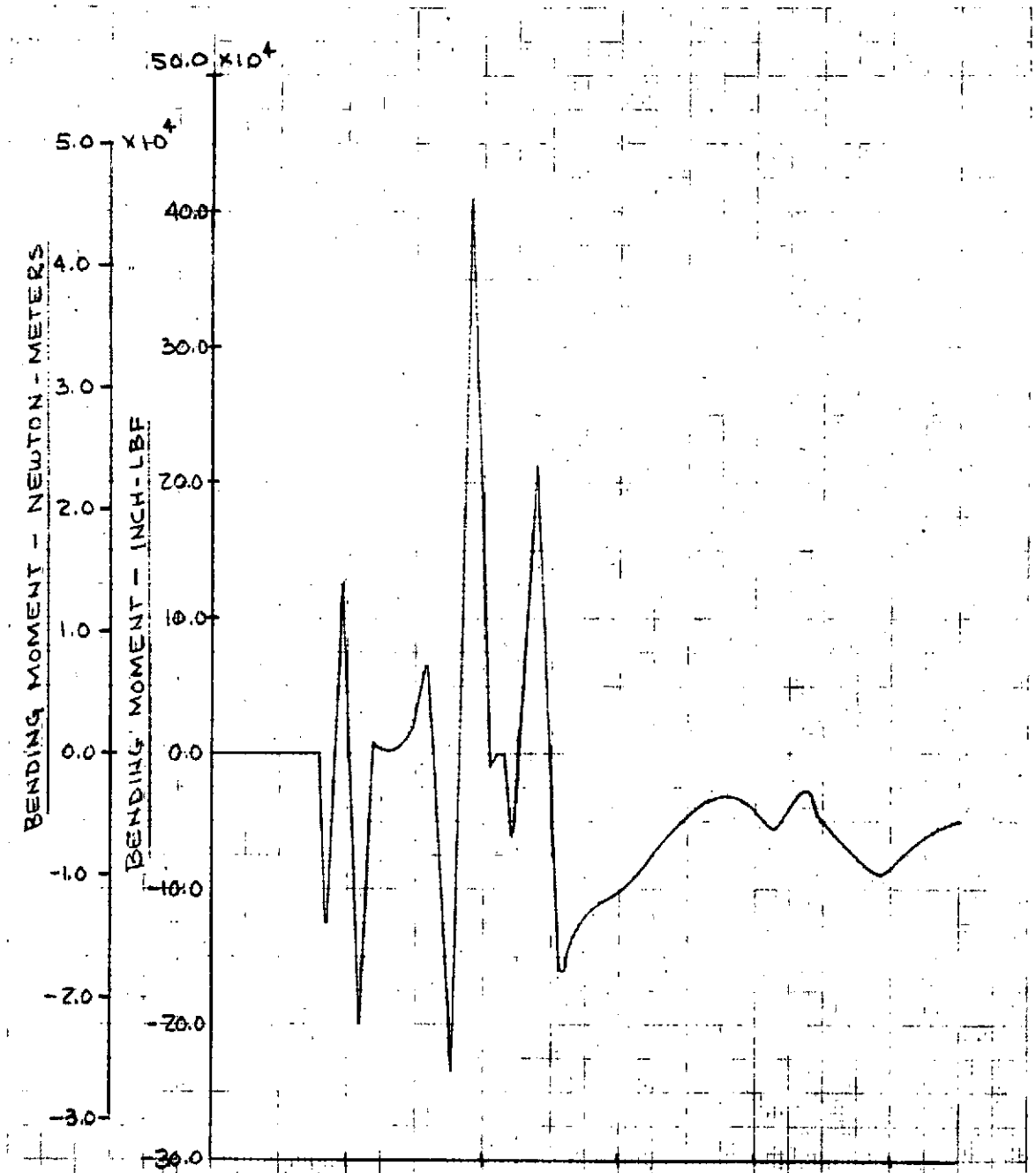

FIG. 21 - SHROUD LONGITUDINAL BENDING MOMENT AT STATION 274 VS. TIME (EARLY OFF CASE; 1500 LBF (6675 NEWTONS) BRAKE CABLE TENSION; 8.4 DEG (.1466 RAD) NET ANGLE

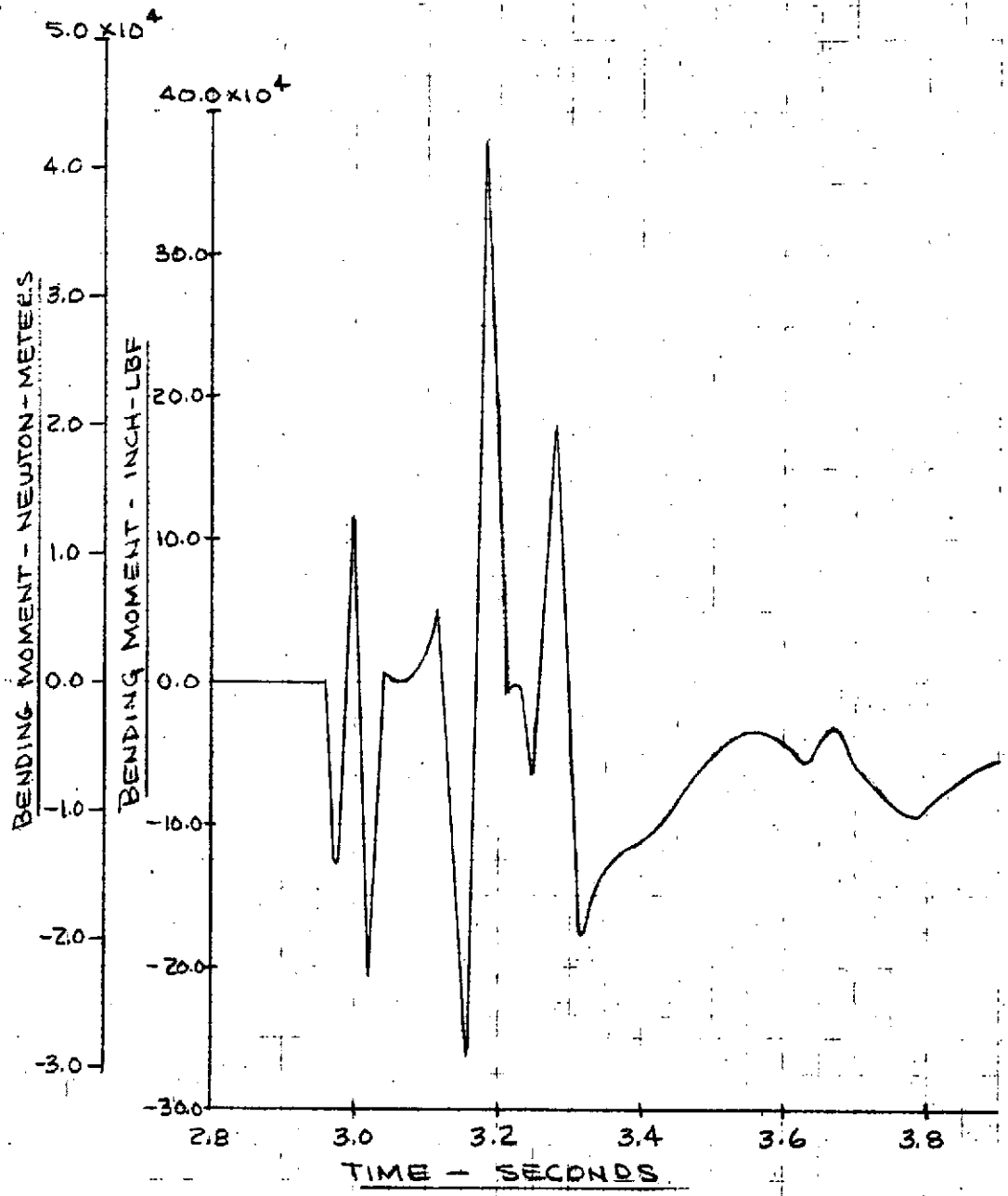

FIG. 22 - SHROUD LONGITUDINAL BENDING MOMENT AT STATION 250 VS. TIME (EARLY OFF CASE; 1500 LBF (6675 NEWTONS) BRAKE CABLE TENSION; 8.4 DEG (.1466 RAD) NET ANGLE

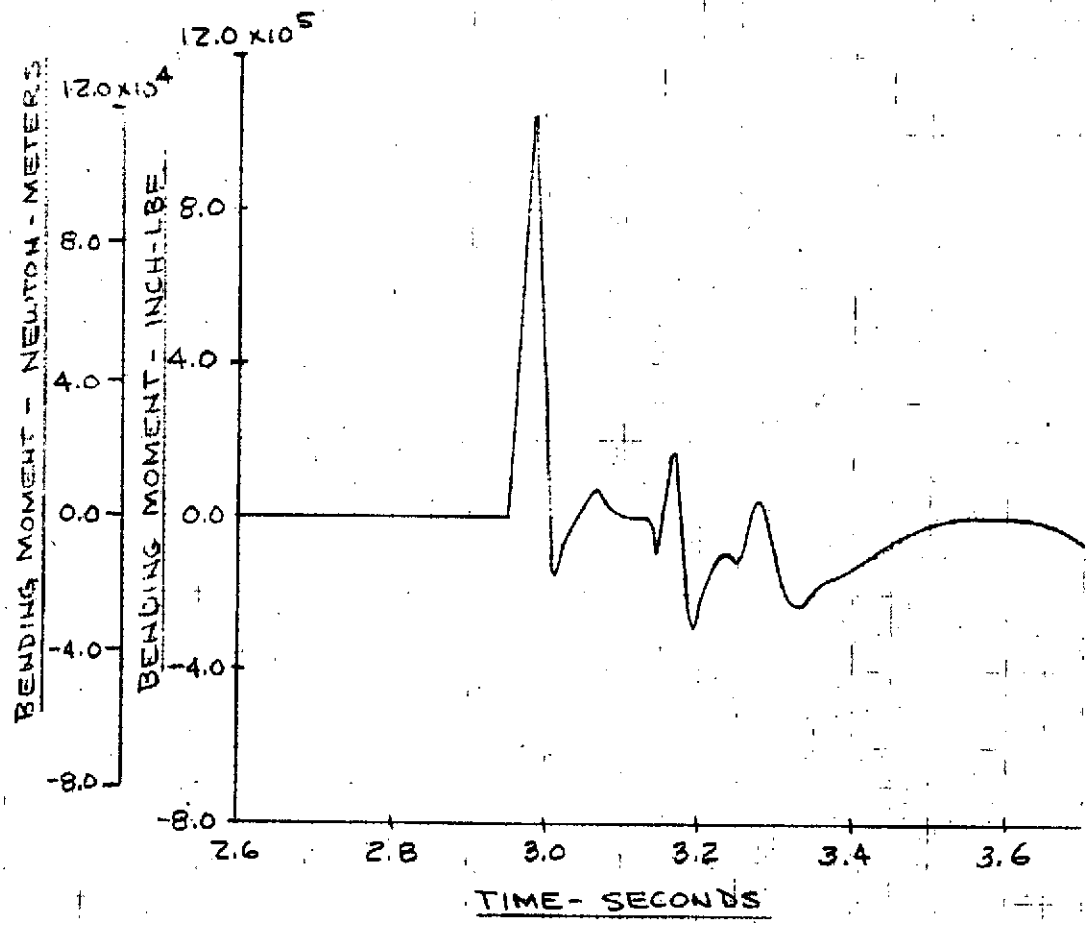

FIG. 23- SHROUD LONGITUDINAL BENDING MOMENT AT STATION 274 VS. TIME (LATE OFF CASE; 1500 LBF (6675 NEWTONS) BRAKE CABLE TENSION; 8.4 DEG (.1466 RAD.) NET ANGLE

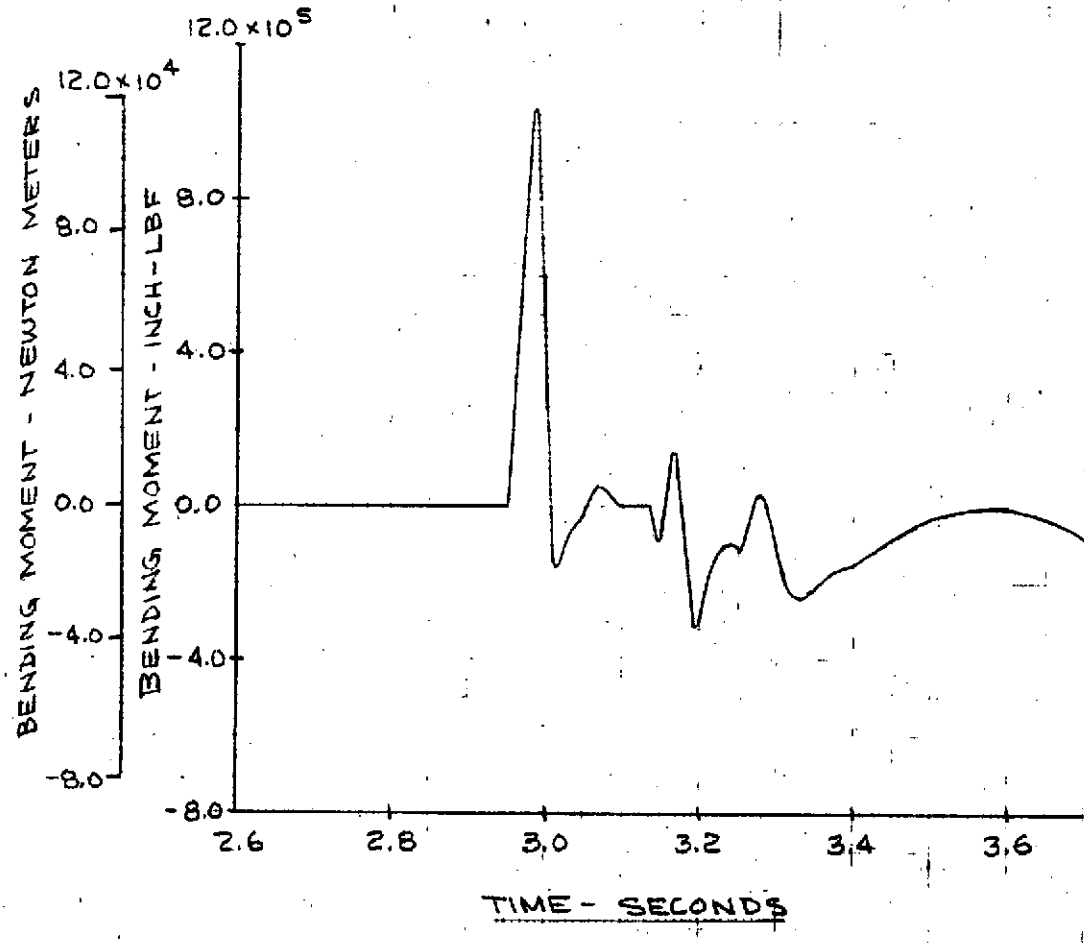

FIG. 24 SHROUD LONGITUDINAL BENDING MOMENT AT STATION 250 VS. TIME (LATE OFF CASE; 1500 LBF (6675 NEWTONS) BRAKE CABLE TENSION; 8.4 DEG (.1466 RAD.) NET ANGLE

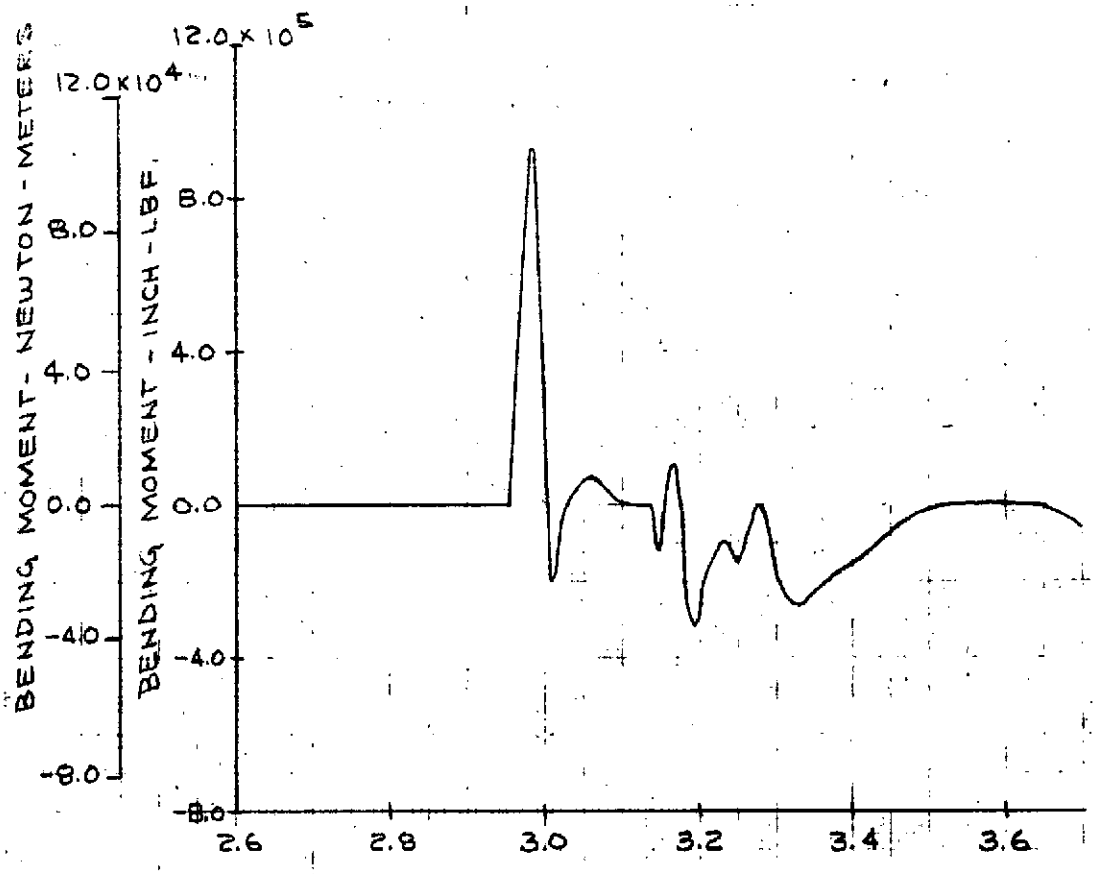

FIG 25 - SHROUD LONGITUDINAL BENDING MOMENT AT STATION 344 VS. TIME (LATE OFF CASE; 1500 LBF (6675 NEWTONS) BRAKE CABLE TENSION; 8.4 DEG (.1466 RAD.) NET ANGLE

BY ..... DATE ..... SUBJECT ..... SHEET NO. ..... OF .....
CHKD BY ..... DATE ..... JOB NO. .....

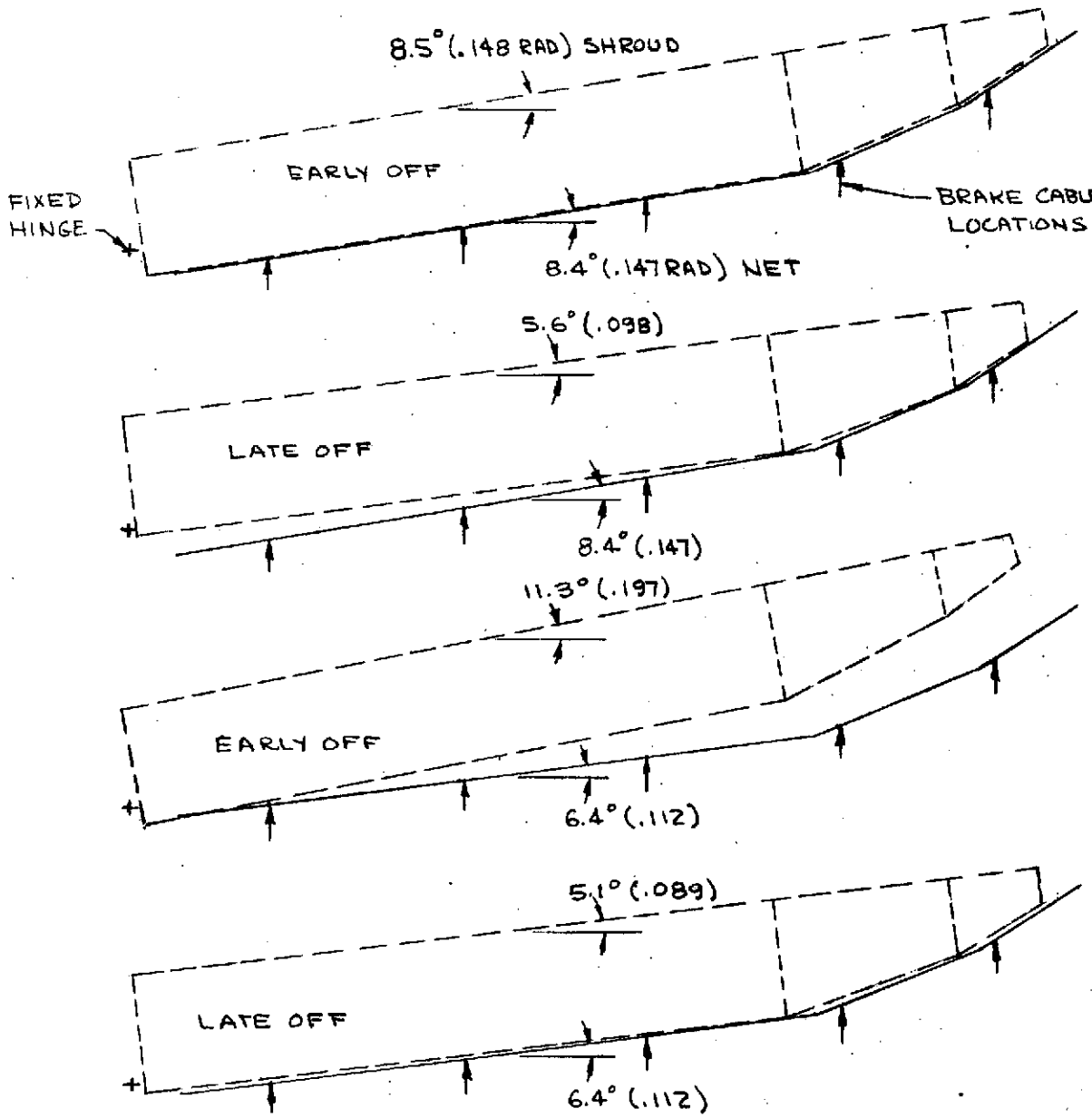

FIG. 26 - SHROUD INITIAL CONTACT ANGLE FOR THREE NET ANGLES.

BY..... DATE..... SUBJECT..... SHEET NO..... OF.....

CHK'D. BY..... DATE..... JOB NO.....

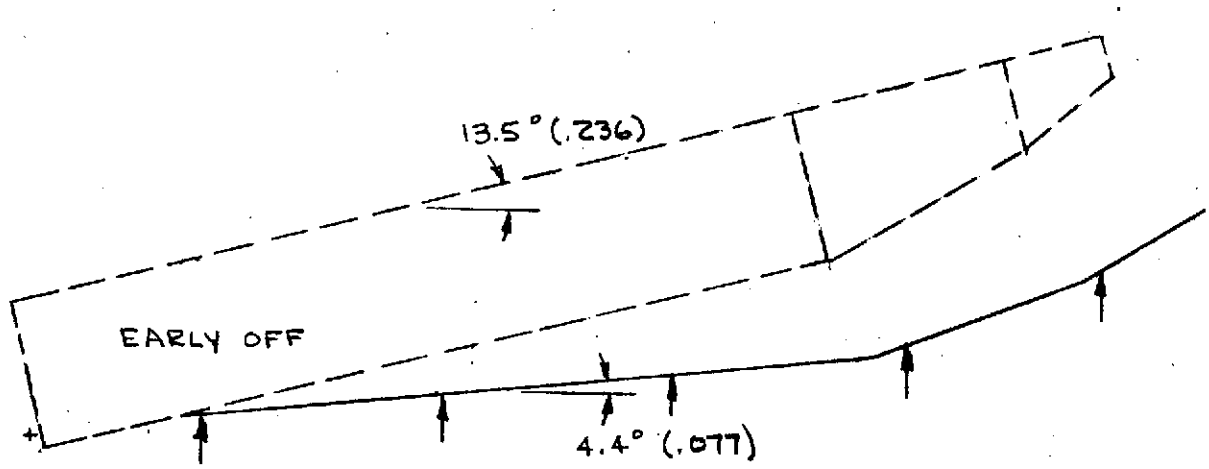

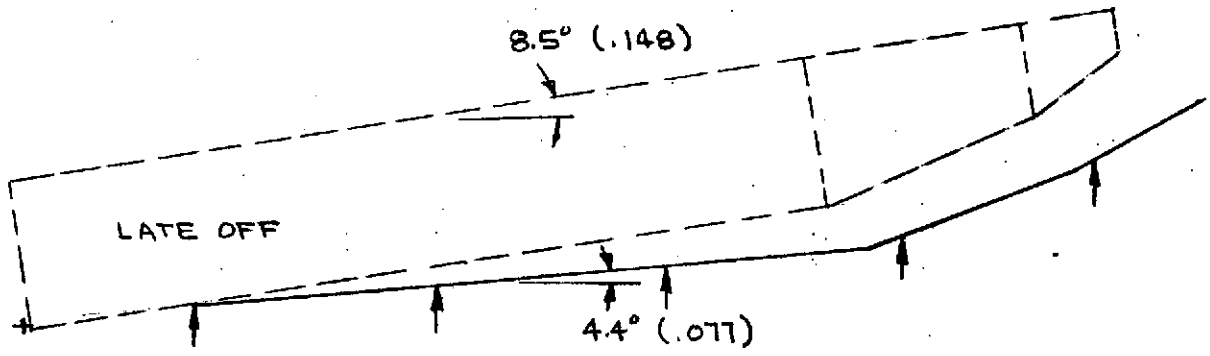

FIGURE 26a(CONT'D)

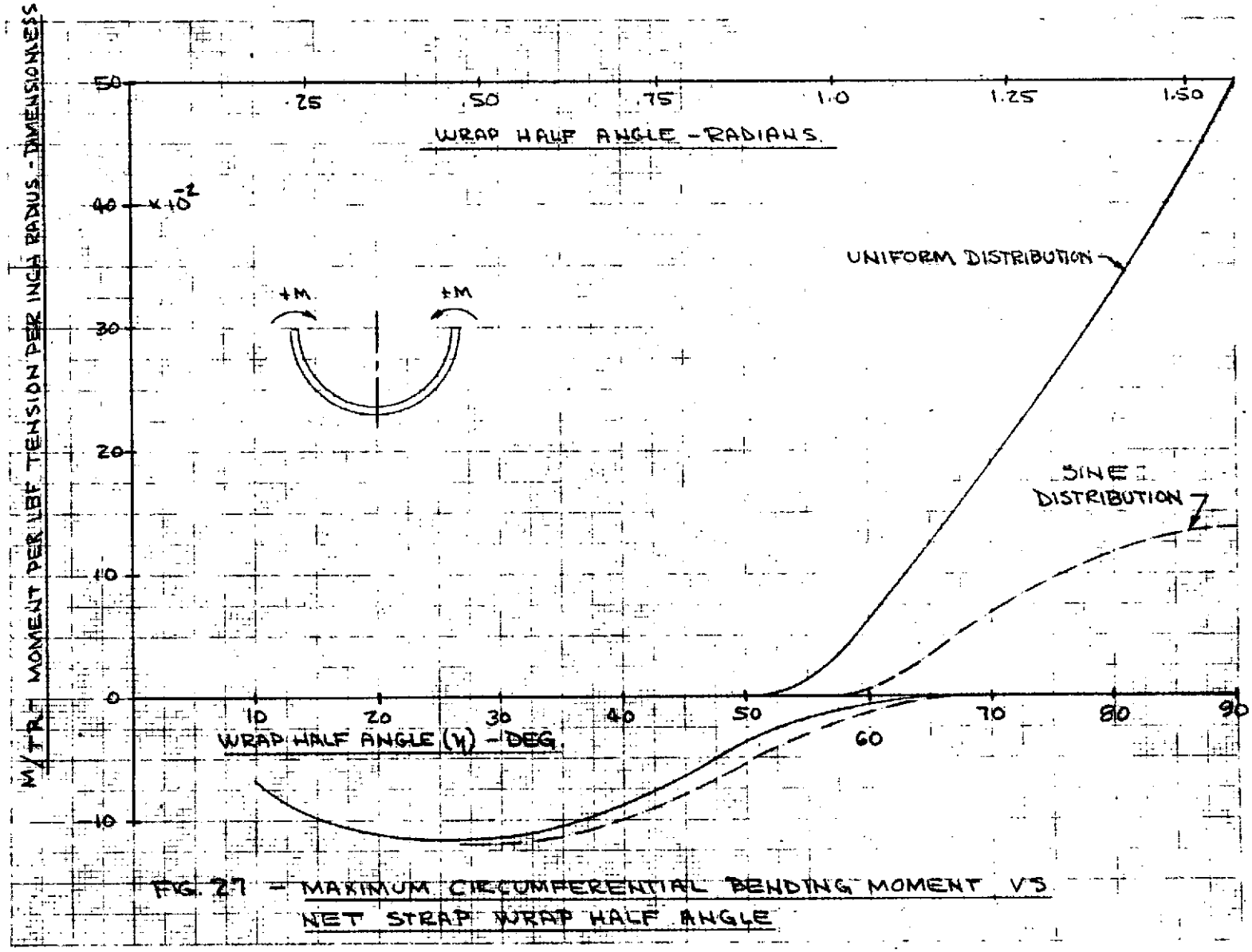

FIG. 27 - MAXIMUM CIRCUMFERENTIAL BENDING MOMENT VS NET STRAP WRAP HALF ANGLE

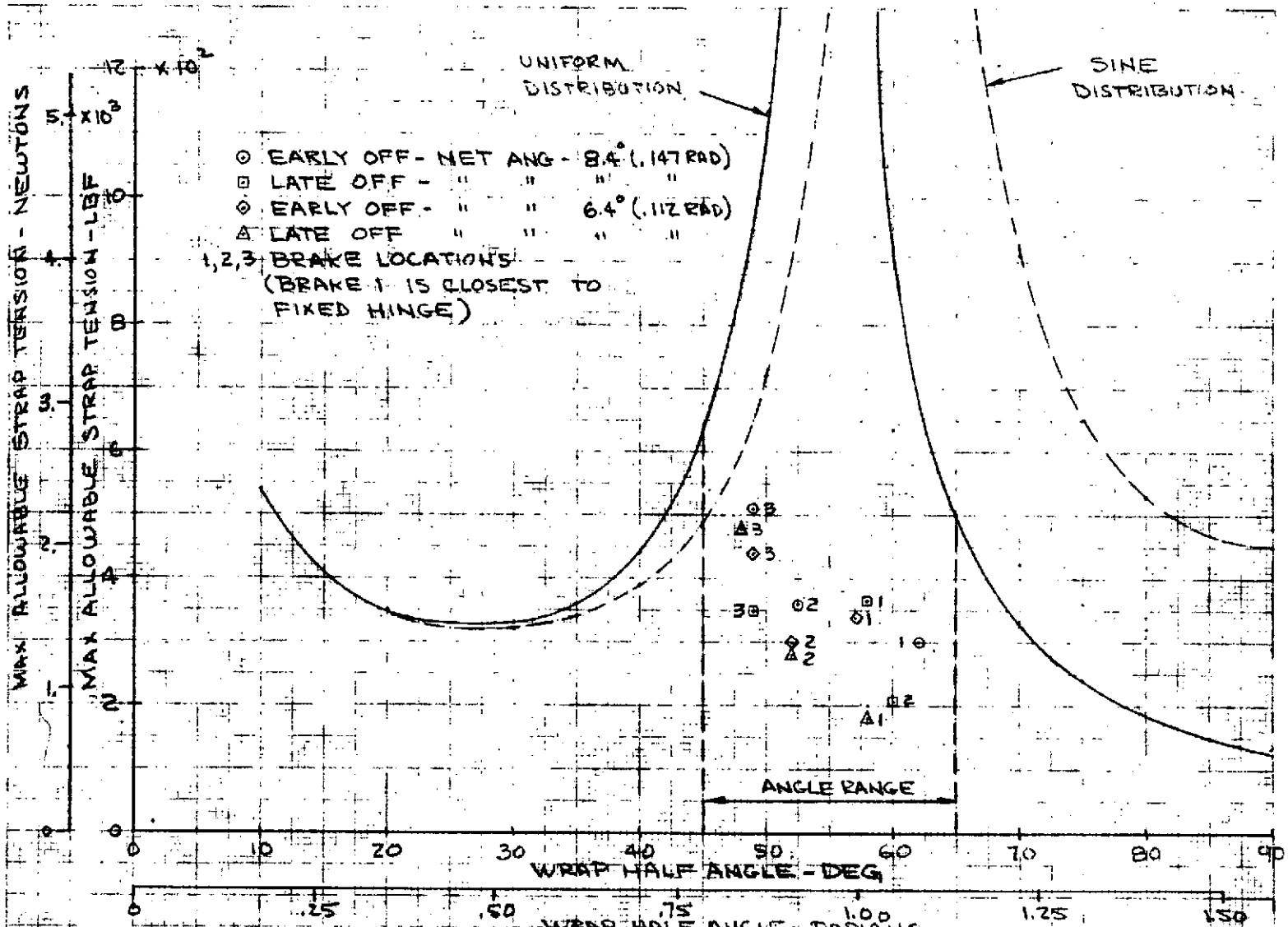

FIG. 28 - MAX. ALLOWABLE STRAP TENSION VS. WRAP HALF ANGLE, R=84.5 IN. (2.14 m)

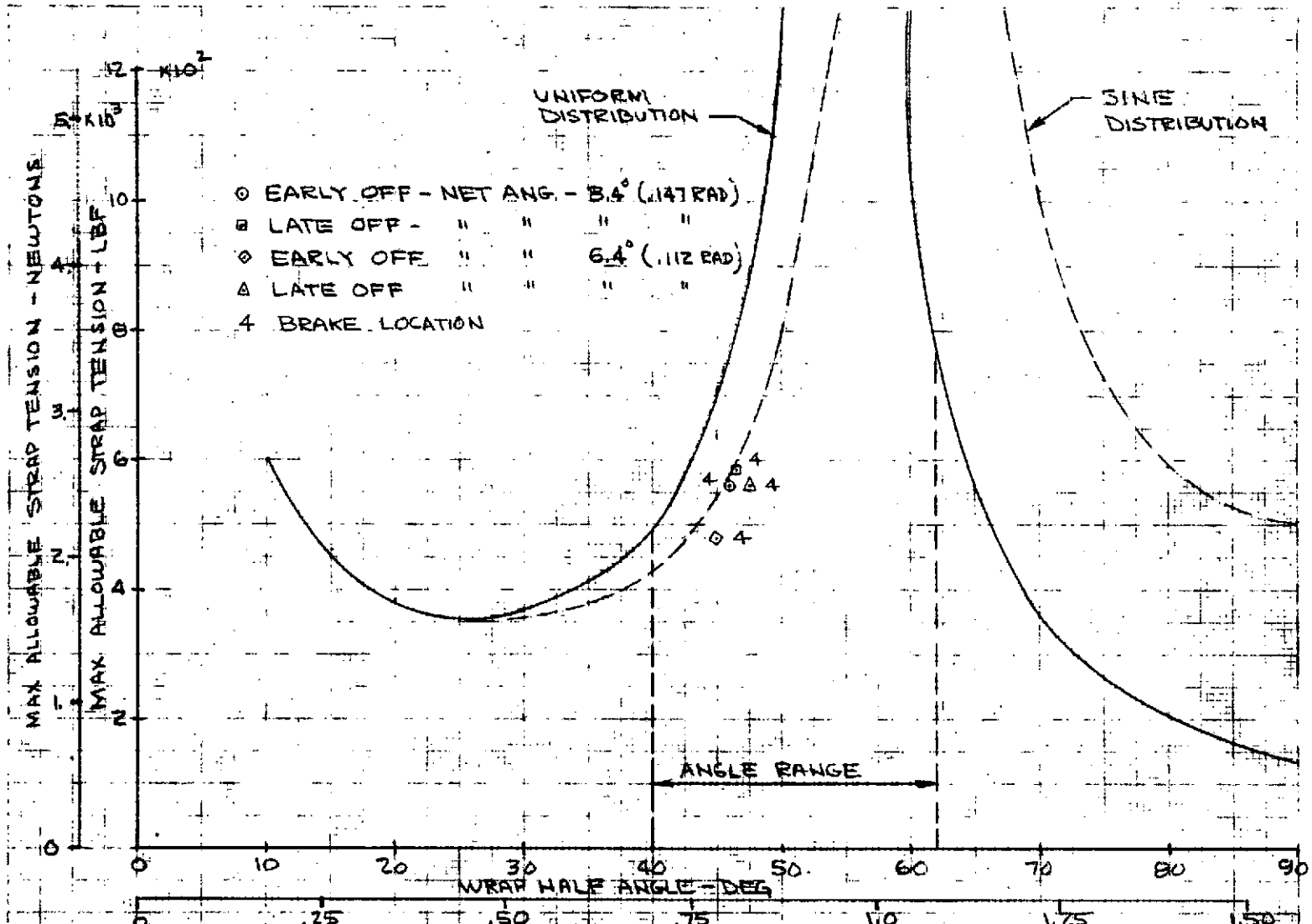

FIG. 29 - MAX. ALLOWABLE STRAP TENSION VS. WRAP HALF ANGLE, R=76 IN (1.93 m.)

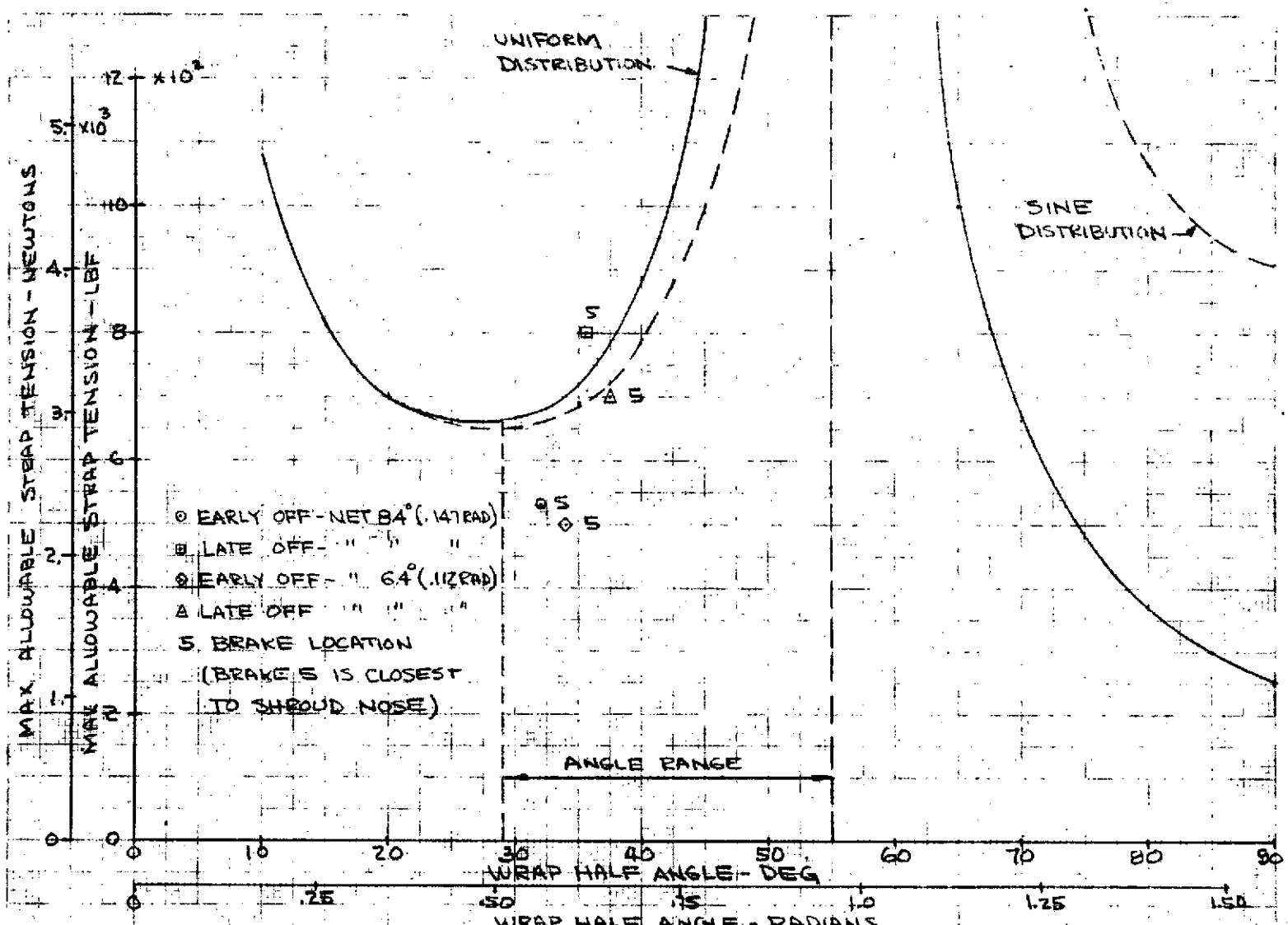

FIG. 30 - MAX ALLOWABLE STRAP TENSION VS WRAP HALF ANGLE, R = 42 IN. (1.068M)

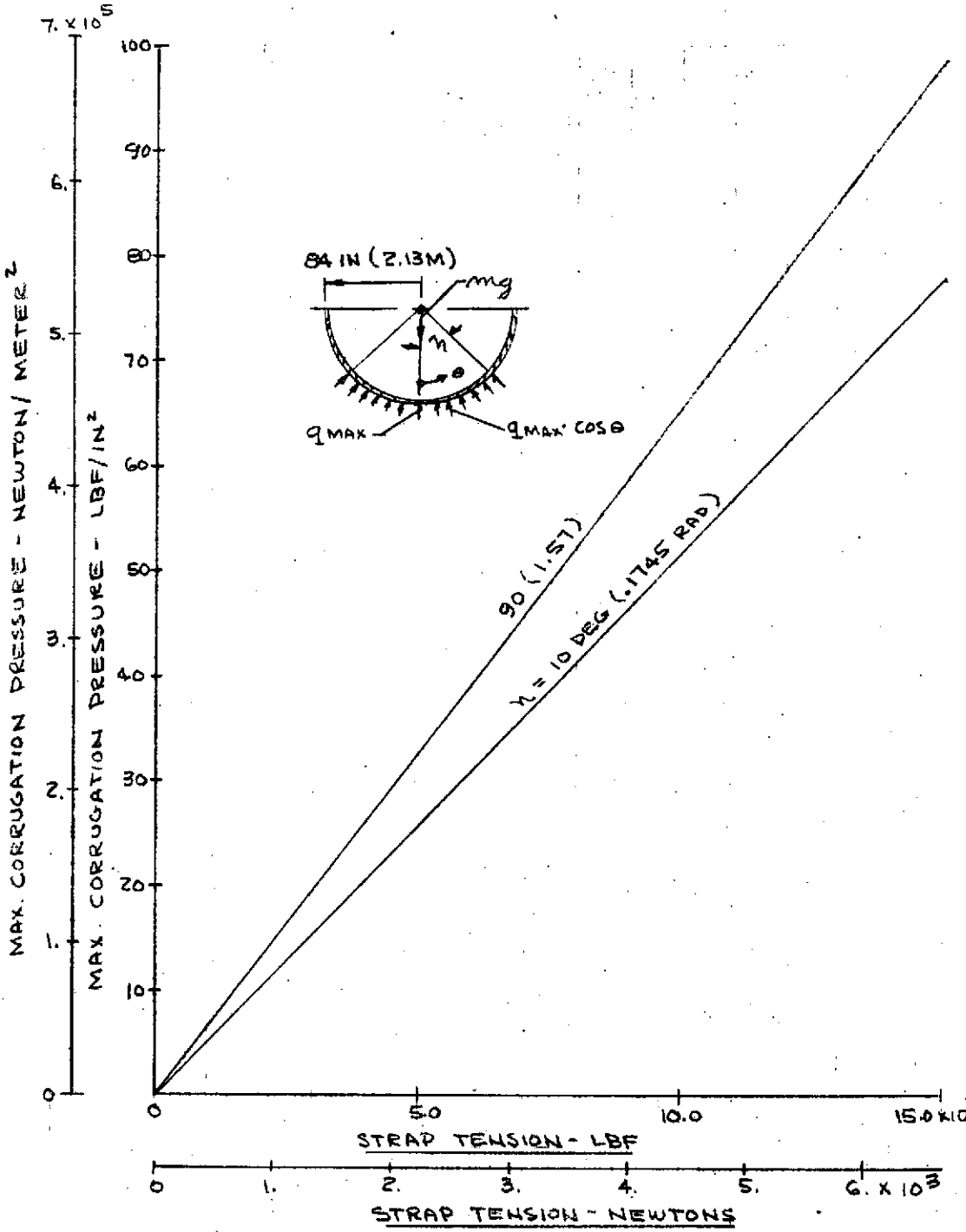

FIG 31 - MAXIMUM CORRUGATION PRESSURE VS NET STRAP TENSION FOR TWO WRAP HALF ANGLES